Numerical simulation of the turbidity maximum transport in the Gironde estuary (France)

Numerical model
Fine-grained sediment transport
Suspended matter,
Turbulence
Gironde estuary

Modèle numérique
Transport de sédiment fin
Matière en suspension
Turbulence
Estuaire de la Gironde

Zhan Hua LI [1], Kim Dan NGUYEN [2], Jean-Claude BRUN-COTTAN [3] and Jean-Marie MARTIN

Institut de Biogéochimie Marine, URA C.N.R.S 386, URM Ifremer 6,
École Normale Supérieure, 1, rue Maurice Arnoux, 92120 Montrouge, France

[1] New address : Institute of Mechanics, Chinese Academy of Sciences, 15, Zhong Guan Cun Road, Beijing 100080, China.

[2] Author for correspondence.

[3] New address : Centre de Géomorphologie et Transports de Surface C.N.R.S., 24, rue des Tilleuls, 14000 Caen, France.

Received 29/06/93, in revised form 30/06/94, accepted 13/09/94

ABSTRACT

A coupled two-dimensional vertical width-integrated hydrodynamic and sediment transport numerical model is presented to simulate the "turbidity maximum" formation and dynamics in the Gironde estuary. A turbulence closure sub-model is used to parametrize the turbulent mixing process. The numerical results of a five-day simulation are compared with field measurements carried out at several locations. The formation and the displacement of the turbidity maximum during one tidal cycle are correctly simulated. The intensity of the "turbidity maximum" is strongly related to the turbulent energy field. The influence of the tidal amplitude on the suspended matter transport is also studied during the simulation.

RÉSUMÉ

Simulation numérique du bouchon vaseux dans l'estuaire de la Gironde

Un modèle numérique 2D vertical, intégré sur la largeur, couplant l'hydrodynamique et le transport sédimentaire, est présenté pour simuler le «bouchon vaseux» dans l'estuaire de la Gironde. Un sous-modèle de fermeture de la turbulence est utilisé pour paramétriser les échanges turbulents. Les résultats numériques obtenus pour une simulation de cinq jours, sont comparés à ceux obtenus par des mesures directes en plusieurs sites. La formation et le déplacement du « bouchon vaseux » au cours d'un cycle de marée est bien décrit. Sa concentration est fortement reliée au champ de l'énergie turbulente. L'influence du coefficient de marée sur le transport sédimentaire a aussi été étudiée.

Oceanologica Acta, 1994. **17**, 5, 479-500.

INTRODUCTION

The transport of fine-grained sediment is very important to the prediction of the flux of pollutants in estuaries and the design of dredging strategies for navigation channels. The main feature of fine-grained sediment transport in macrotidal estuaries is the "turbidity maximum", a phenomenon that has long been observed in various macrotidal estuaries (Baumgartnen (1836-1844) ; Glangeaud, 1939; Inglis and Allen, 1957). This turbidity maximum, characterized by a high suspended matter concentration zone in the estuary, moves with the tide and its location depends on the river flow. The residence time of the particles that constitute the maximum is at least several months, and probably of the order of years for the Gironde estuary (Martin *et al.*,1986).

Turbidity maximum transport in estuaries, a complex dynamic process which involves various time scales (Dyer, 1988), depends on tidal dynamics, river discharge and the erosion and settling of sediment, as well as the erodibility of the bottom sediment. The time scales consist of

half-day (short lunar tidal period), two-week (long lunar tidal period) and seasonal scales (influence of river discharge). The Gironde estuary (France) is a partially mixed and macrotidal estuary (Allen, 1973), with well-developed turbidity maximum extending for 20-60 km of its length as a permanent feature. Total Suspended Matter (TSM) concentration can exceed 50 $g \cdot l^{-1}$ near the bottom (Allen, 1973). Some hypotheses have been advanced in the past to explain the formation and the displacement of the turbidity maximum. They mainly involved the role of the salt water motion at the bottom of the estuary and the tide-averaged residual circulation (introduction of a so called "null point"). The role of the flocculation processes at the fresh and salt water interface, and more recently, the effects of the global dynamic interactions have also been invoked.

Mathematical models of the TSM and mud transport in estuaries have been developed since the early 1970s: for instance, Odd and Owen (1972) for the Thames estuary; Du Penhoat and Salomon (1979) for the Gironde estuary, Rodger and Odd (1985) for the Brisbane estuary and Le Hir and Karlikow (1991) for the Loire estuary. In the most basic and commonly used models, the movement of mud in an estuary is considered to be governed by a cycle of erosion, transport in suspension with vertical mixing, settling and deposition. Most of the advances in recent studies have involved refining the physical processes: the representation of the processes of erosion and deposition of sediment (Falconer and Owens, 1990); and the simulation of the effect of sediment-induced stratification on the bottom boundary layer dynamic and on the erosion processes (Sheng and Villaret, 1989).

The aim of this paper is to describe a two-dimensional vertical model that simulates turbidity maximum behaviour in the Gironde estuary, to show the effect of some important hydrodynamic and sedimentological processes and to improve the simulation of turbulent vertical mixing by introducing a turbulence closure sub-model.

MAIN FEATURES OF THE GIRONDE ESTUARY

The Gironde estuary, located in southwestern France, is a product of the confluence of the Garonne and Dordogne rivers (Fig.1). Its geometry from Bordeaux to Pauillac, except for islands such as the Ile Verte, is considered to be regular. The water-surface width is about 2-3 km and the depth 6-8 m in the navigation channel. However, from Pauillac to the mouth, the geometry becomes more com-

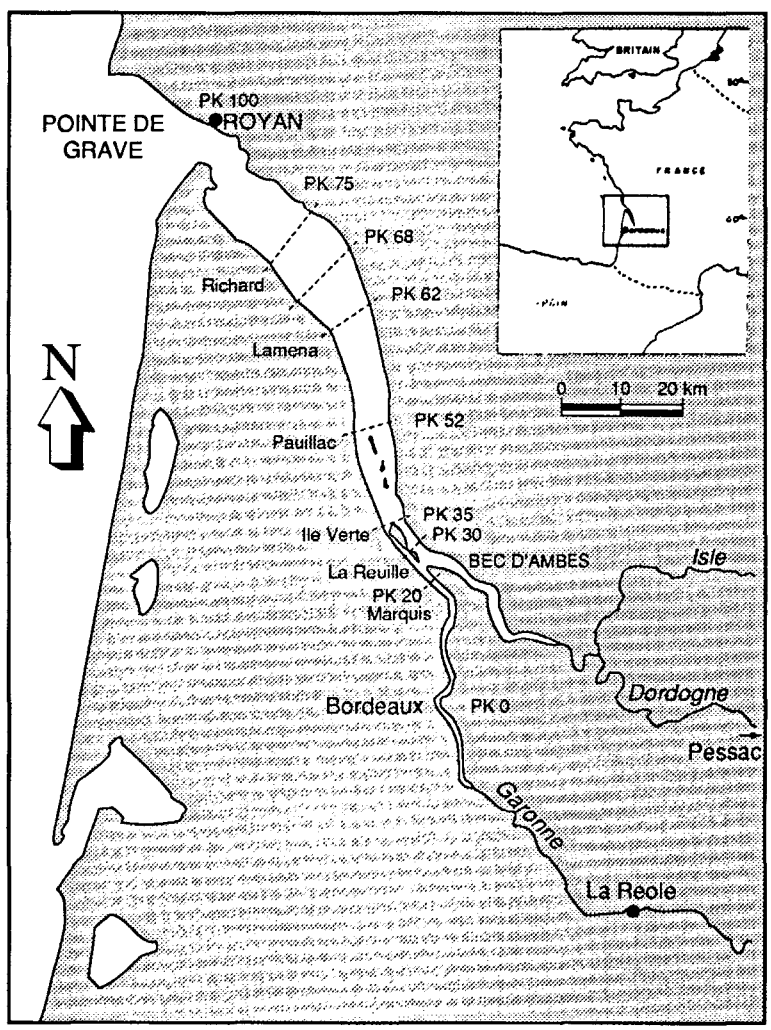

Figure 1

Chart of the Gironde estuary showing the sampling sections (PK: Kilometres downstream from Bordeaux).

plex due to an increase of width and the presence of the Saintonge channel on the right bank. The width ranges from 4 km at Pauillac to 14 km at Richard. The depth is 10 m in the navigation channel in this region. From Richard to the mouth of the estuary, the bottom depth increases from 10 m to 30 m over a distance of 10 km.

The total drainage area of the estuary is about 8.10^4 km^2, and the annually-averaged river discharge (1961-1970) amounts to 760 m^3.s^{-1} (Jouanneau and Latouche, 1981). Seasonal variations in river flow occur with maximum values, usually in January (1,500 m^3.s^{-1} monthly mean), and minimum values in August (200 m^3.s^{-1}) (Jouanneau and Latouche, 1981). The estuary is partially mixed and macrotidal, with a 12 hour and 25 minutes tidal lunar period and a tidal amplitude of 1.5 to 5 m at the mouth. Tide effects are felt up to 150 km upstream from the mouth during periods of low river discharge, whilst the upper limit of the salinity intrusion is about 75 km upstream for low river discharge, and 40 km for high river discharge (Allen, 1973). The annually-averaged solid discharge to the estuary (1959-1965) is about 2.17 10^6 tons, two-thirds of which are contributed by the Garonne river (Migniot, 1971).

The sedimentological structure of the bottom varies from the mouth to the upstream boundaries of the tidal intrusion in the Garonne and Dordogne rivers.

– At the mouth of the estuary, the bottom is covered by sand.

– From Richard (25 km upstream from the mouth) to Bordeaux, a "fluid mud" layer, constituted by silt and mostly by clay minerals, can cover the bottom in patches, mainly in the navigation channel. These patches are mostly 10 to 20 km long, and up to 2-3 metres thick. Close to Bordeaux when the river flow is low, they drift seaward to Richard when the river flow is high.

– From Bordeaux to the upstream boundary (70 km upstream from Bordeaux) and for the part of the Dordogne river taken into account in the computed domain, the river bed constituted by non-consolidated soft mud with patches of sand.

River solid discharge combined with macro-tidal conditions causes the formation of a well-developed "turbidity maximum". This turbidity maximum and the fluid mud are located in the same area of the estuary, and can be considered as a coupled system, the maximum total mass of which is of the order of 2-5 10^6 tons (close to the annual solid river discharge). When the turbidity maximum is fully developed, during the high tidal amplitude period, the total mass of the fluid mud in the estuary decreases or disappears. The reverse phenomenon occurs during the small tidal amplitude period. Within the turbidity maximum, the TSM concentration increases from the top to the bottom of the water column. When this concentration exceeds 150 g.l^{-1}, the top of the fluid mud layer is reached, with the concentration corresponding to a change of the mechanical properties of the fluid from Newtonian to non-Newtonian. The concentration of the fluid mud layer varies from 150 g.l^{-1} at the top to 400 g.l^{-1} at the bottom. With a greater concentration, the consolidated bottom is considered as reached. Some experiments with radio-tracers (Jouanneau and Latouche, 1981) show ii that the fluid mud has no horizontal velocity, ii its displacement, when the river flow varies, is due to the displacement of the turbidity maximum; iii material resuspended from the fluid mud then settles at a new location. The top of the fluid mud layer is thus considered as the mathematical bottom boundary. Only the resuspended sediment transport is described in this paper. However, when determining the bottom conditions of the erosion, some mechanical properties of the fluid mud are taken into account (see section : sedimentological parameters).

MATHEMATICAL AND NUMERICAL BACKGROUND

The basis of the model described here is a two-dimensional width-integrated model first proposed by Nguyen (1987) to simulate estuarine water circulation. The sigma-coordinate system transformation on the z axis is thus used in order to take into account significant variations of the bottom topography and the tidal water surface when setting the computing point-grid (the number of grid points on the vertical remains constant). The computational domain includes the Garonne and Dordogne rivers. A numerical technique to couple the confluence of the two rivers with the Gironde estuary is then used. A turbulence closure sub-model is introduced to calculate the turbulent viscosity coefficients.

Governing equations

The governing equations are the Navier-Stokes ones, integrated over the whole width, with the following hypothesis: (i) Hydrostatical approximation for the vertical distribution of pressure; (ii) Boussinesq's approximation for the density distribution so that a constant reference density ρ_0 may, except for the buoyancy term, be substituted for the water density ρ without any serious errors for all terms of the governing equation; (iii) Lateral variation of the mass and momentum distributions are negligible.

Let the coordinate origin be at the mean water level. The x axis is horizontal pointing landward and the z coordinate is taken positive upward (Fig. 2). b is the width of the

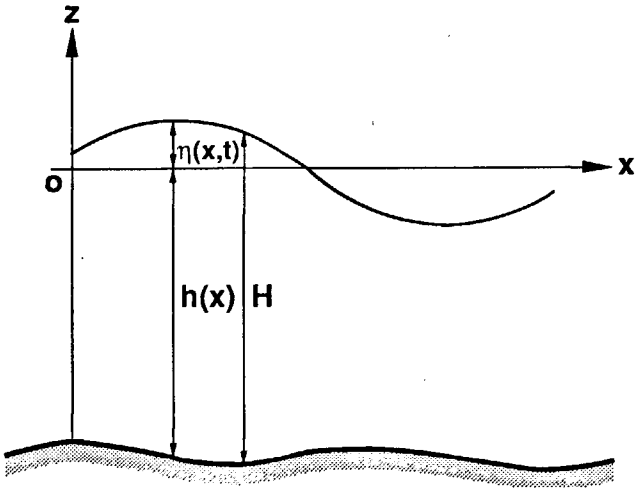

Figure 2

Coordinate system.

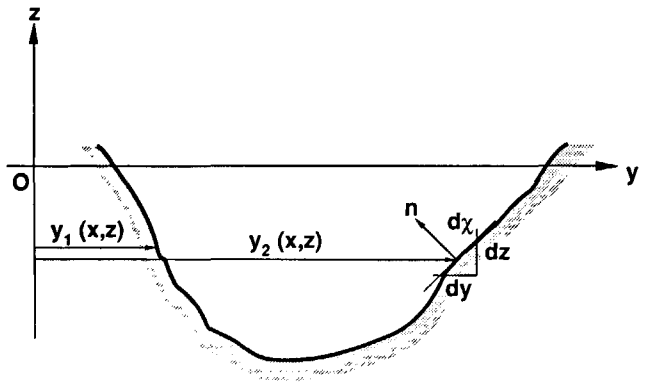

Figure 3

Transverse coordinate system used for the side-wall shear stress calculation.

estuary; u, w the width-averaged velocity components in the x and z axis respectively; S the salinity; C the turbidity. Hence, the governing equations are as follows:

Continuity equation:

$$\frac{\partial(bu)}{\partial x}+\frac{\partial(bw)}{\partial z}=0 \tag{1}$$

Momentum equation:

$$\begin{aligned}&\frac{\partial(bS)}{\partial t}+\frac{\partial(buS)}{\partial x}+\frac{\partial(bwS)}{\partial z}\\&=-gb\frac{\partial\eta}{\partial x}-\alpha gb(\eta-z)\frac{\partial S}{\partial x}\\&+\frac{\partial}{\partial z}\left(bK_z\frac{\partial u}{\partial z}\right)+\frac{\partial}{\partial x}\left(bK_x\frac{\partial u}{\partial x}\right)-F_\tau\end{aligned} \tag{2}$$

Salinity transport equation:

$$\begin{aligned}&\frac{\partial(bS)}{\partial t}+\frac{\partial(buS)}{\partial x}+\frac{\partial(bwS)}{\partial z}\\&=\frac{\partial}{\partial z}\left(bK_{zs}\frac{\partial S}{\partial z}\right)+\frac{\partial}{\partial x}\left(bK_{xs}\frac{\partial S}{\partial x}\right)\end{aligned} \tag{3}$$

Sediment transport equation:

$$\begin{aligned}&\frac{\partial(bC)}{\partial t}+\frac{\partial(buC)}{\partial x}+\frac{\partial[b(w-w_s)C]}{\partial z}\\&=\frac{\partial}{\partial z}\left(bK_{zc}\frac{\partial C}{\partial z}\right)+\frac{\partial}{\partial x}\left(bK_{xc}\frac{\partial C}{\partial x}\right)\end{aligned} \tag{4}$$

where η is the water surface elevation; $w_s > 0$ the particle settling velocity; K_x the horizontal momentum dispersion coefficient; K_z the vertical turbulent viscosity coefficient; K_{xc}, K_{xs} the horizontal mass diffusion coefficients; K_{zc}, K_{zs} the vertical turbulent diffusion coefficients. The subscripts s and c denote salinity and turbidity, respectively ; x and z represent the directions.

The friction term F_τ in equation (2), along the two lateral sides of a river cross-section is defined as:

$$F_\tau=\int_{y_1}^{y_2}\frac{1}{\rho}\frac{\partial\tau_{xy}}{\partial y}dy=\frac{g}{Ch^2}u|u|\left(\left|\frac{\partial\chi}{\partial z}\right|_{y_1}+\left|\frac{\partial\chi}{\partial z}\right|_{y_2}\right) \tag{5}$$

where τ_{xy} is the side-wall stress; $\frac{\partial\kappa}{\partial z}$ the lateral-side slope in the z direction of the cross-section (Fig. 3); Ch is the Chezy coefficient.

Estuarine circulation is not completely driven by tidal forcing. Some non-tidal processes have an important effect and must be taken into account, the principal ones among them being: river discharge; density gradients; turbulent energy exchanges in fluid flows; wind stress on the water surface; and bottom and lateral-wall friction. The complexity of the topography and the morphology precludes the simple use of a rectangular geometry for each cross-section in the estuary to calculate the bottom and side-wall friction. In the proposed model, the width of every cross-section thus depends on the x and z coordinates. The maximum water depth Hmax(x) and the relative width bmax(x,z) are given. The instantaneous width b(x,z) is calculated by a linear interpolation corresponding to the real water depth (Fig. 4).

Boundary Conditions

At the water surface

For the momentum equation, the shear stress τ_w at the water surface, due to the wind effect, implies:

$$\rho K_z\left(\frac{\partial u}{\partial z}\right)_{z=\eta}=\tau_w \tag{6}$$

For the salt transport equation,

$$K_{zs}\left(\frac{\partial S}{\partial z}\right)_{z=\eta}=0 \tag{7}$$

For the TSM transport equation,

$$\left(K_{zc}\frac{\partial C}{\partial z}+w_sC\right)_{z=\eta}=0 \tag{8}$$

At the bottom

The bottom shear stress can be expressed as follows:

$$\tau_b=\rho K_z\left(\frac{\partial u}{\partial z}\right)_{z=-h} \tag{9}$$

Near the bottom, because of the boundary layer effects, a direct simulation of the current velocity and the bed shear stress would imply an excessive local refinement of the computing grid. Moreover, the velocity profile in the tur-

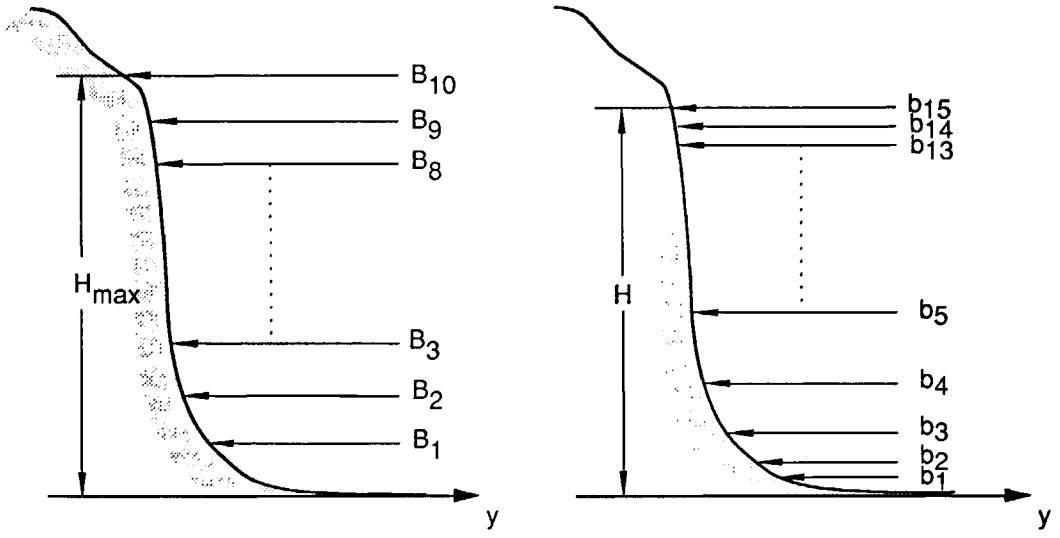

Figure 4

Schematic cross-section of the estuary width as a function of x and z. (For each section of the estuary, the width at the surface (B_{10}) corresponds to the maximum water depth (Hmax). Hmax is divided in 10 layers of the same thickness. The real width at each point of the mesh (b_k, k = 1, n_z where n_z is the point grid number over the vertical), related to the real water depth H, is interpolated based on the corresponding layer.)

bulent boundary layer is known as a logarithmic law (Dyer, 1986). The current velocity u_a at point a very near the bottom is thus expressed as follow (Bradshaw, 1978):

$$\frac{u_a}{u_*} = \frac{1}{K}\mathrm{Ln}\left(\frac{z_a}{z_0}\right) + C_1 \qquad (10)$$

where z_a is the distance from the point a to the bottom, K is the von Karman constant (= 0.4), u_* the friction velocity, z_0 the bottom roughness and C_1 an integration constant (= 5). u_* is unknown, but from the derivative of u with respect to z, one obtains:

$$\left.\frac{\partial u}{\partial z}\right|_{z=-h} = \frac{u_a}{K z_a C_2}$$

$$\text{with } C_2 = \frac{1}{K}\mathrm{Ln}\left(7.7\frac{z_a}{z_0}\right) \qquad (11)$$

This expression is applied as the boundary condition for the momentum equation. z_0 is calculated with the formula given by Ramette (1981): $z_0 = H(26.4/Ch)^8$. This method was used by Sauvaget (1987), to deal with the boundary condition in an estuarine flow modelling.

For the salt transport equation:

$$K_{zz}\left(\frac{\partial S}{\partial z}\right)_{z=-h} = 0 \qquad (12)$$

For the TSM transport equation:

$$\left(-K_{zz}\frac{\partial C}{\partial z} - w_s C\right)_{z=-h} = F_e - F_d \qquad (13)$$

F_e and F_d are the erosion and deposition flux functions, integrated on the width b.

At the open boundaries

At the estuary mouth, the water elevation is permanently given by the recorded values of the tidal elevation at the locality known as "Pointe de Grave". At the two upstream ends, the river discharges of the Garonne and the Dordogne, *i.e.* at la Réole and Pessac respectively, are provided by the recorded data (IGBA, 1975).

Regarding the salinity at the mouth, values based on measured data and revised, according to tidal amplitudes, are used. At the upstream ends, the salt concentration value is assumed to be 0.1 g l^{-1}, which corresponds to the freshwater content in salts; the sea-water salinity effect is null.

Based on the annually-averaged river solid discharges of 2.2 10^6 tons and the river discharges of 30 Gm^3, the turbidity at the upstream ends is assumed: 0.03 g l^{-1} for the Garonne river and 0.02 g l^{-1} for the Dordogne river. At the mouth, the turbidity of the seawater is set to 10 mg l^{-1} during the flood, while the turbidity is calculated by the model during the ebb.

Sedimentological parameters

In the Gironde estuary, the fine-grained sediments are for the most part cohesive. The main parameters governing the erosion flux F_e and the deposition flux F_d of TSM on the bottom are the critical erosion shear stress τ_{ce}, the erosion flux constant M and the critical bottom deposition shear stress τ_{cd}. The vertical flux F_e of the eroded sediment is calculated by using the formula of Partheniades (1962):

$$F_e = M\left(\frac{\tau_b}{\tau_{ce}} - 1\right) \qquad (14)$$

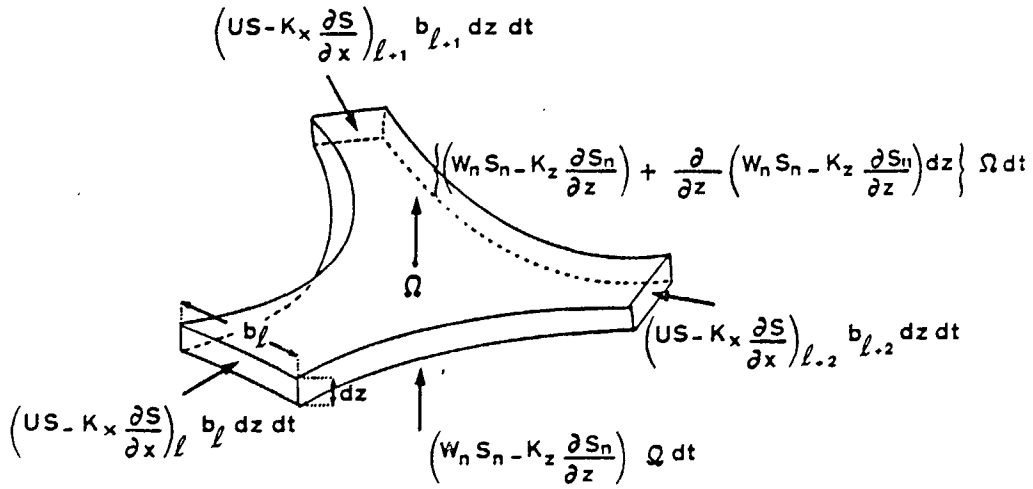

Figure 5

Conservation of the salt mass in the confluent node.

The deposition flux F_d of the TSM is calculated using the formula of Einstein-Krone (1962):

$$F_d = w_s C\left(1 - \frac{\tau_b}{\tau_{cd}}\right) \tag{15}$$

When $\tau_b \geq \tau_{ce}$, sediment erosion occurs. The eroded sediment flux is proportional to the constant M. When $\tau_b \leq \tau_{cd}$, TSM deposition occurs.

Numerous results of laboratory measurements, reviewed by Metha (1988), showed that, under steady and turbulent flows, the rate of deposition depends mainly on the flow conditions, the TSM concentration and the nature of the sediment surface, while the rate of erosion is determined by the bed properties: the bed shear strength and the state of the sediment consolidation. However, in tidal estuaries, where the tidal currents are usually unsteady and where the bottom is not so flat as in the laboratory, the results coming from laboratory experiments must be used with care.

Measurements in the Gironde have shown that particle size ranges from 2 to 300 µm at the salinity front and that a large fraction (>70%) of the TSM could have a particle size over 100 µm (flocs) (Eisma *et al.*, 1991). It is not reasonable therefore, to calculate the settling velocity based on a unique mean particle diameter. Moreover, in the Gironde estuary, where the concentration near the bottom is very high, particle trajectory interactions occur. The hindered settling phenomenon is obvious. The mean TSM settling velocity w_s is thus not calculated with reference to particle size distribution, but is estimated as a function of the TSM concentration. Following the results given by Thorn (1981), in Metha (1986), w_s used in the calculation is:

$$\left.\begin{aligned} w_s &= K_1 C^n && (C \leq 3\ g.l^{-1}) \\ w_s &= w_{so}(1 - K_2 C)^\beta && (C > 3\ g.l^{-1}) \end{aligned}\right\} \tag{16}$$

where $w_{so} \approx 2.6\ 10^{-3}\ m.s^{-1}$, $K_1 = 0.513$, $n = 1.3$, $K_2 = 0.008$, $\beta = 4.65$. According to this formula, $w_s \approx 2\ mm \cdot s^{-1}$ when $C = 3\ g.l^{-1}$.

Linking condition at the confluence

An equation is used for the conservation of the salt mass at the confluence of the Dordogne and Garonne rivers:

$$\frac{\partial(\Omega_N S_N)}{\partial t} dz + \Omega_N \frac{\partial}{\partial z}(w_N S_N - K_{zs} \frac{\partial S_l}{\partial z}) dz = \sum_{l=1}^{3}\left[u_l S_l + K_{xs} \frac{\partial S_l}{\partial X}\right] b_l dz \tag{17}$$

with Ω_N the horizontal water surface area of the confluence zone, w_N the vertical current velocity, S_N the salinity in the confluence area (independent of x), u_l the longitudinal current velocity and S_l the salinity in each branch l, just outside the confluence zone; the N denotes the confluence variables (Fig. 5). A similar expression is assumed for the turbidity, which means that the erosion and deposition fluxes are neglected at the confluence of the rivers.

Turbulence-closure model

The equation system (1)-(5) is not yet closed because the values of the turbulent viscosities and diffusion coefficients are unknown. A turbulence-closure model which permits the determination of these values, must therefore be introduced.

Some turbulence models applied in the oceanic domain have been proposed, such as empirical formulas of turbulent viscosities (Hamilton, 1975), mixing-length models (Boerick and Hogan, 1977) and more frequently one- or two-equation models (Mellor and Yamada, 1982; Blumberg and Mellor, 1987; Nihoul *et al.*, 1989; Galperin and Mellor, 1990) which are mainly based on the transport equations of the turbulent state parameters. In the mixing-length model, the turbulent viscosity K_z is assumed to be proportional to the mean-velocity gradient and a "mixing-length" scale parameter. In the shear-layer flows as boundary layer flows and jet flows, this model gives very good results. But in some complex situations, *e.g.* recirculating flows or unsteady flows, this model is not very suitable, for two reasons:

– the close link with the velocity gradient in the mixing-length model implies a local equilibrium of the turbulent energy. That means that the turbulent energy is locally dissipated at the same rate as it is produced. The turbulent transport and history effects are thus neglected (ASCE, 1988).

– it is quite difficult to specify the mixing-length distribution. A trial-and-error process is therefore generally required to adjust the mixing-length values, in order to obtain a good agreement between the computed results and the observed ones. There is a lack of universality for these models. In order to overcome the limitation of the mixing-length models, equation models are developed, which consider transport and history effects of the turbulent quantities.

The essence of the one- and two-equation models is: (i) the local state of the turbulence is characterized by several parameters: the kinetic energy k, the energy dissipation rate ε or the length-scale of the turbulence l, the dissipation rateε ε can be expressed: $\varepsilon \sim k^{3/2}/l$; (ii) all these quantities can be considered as scalar ones. They are transported by both the advection, due to the mean motion, and the diffusion related to the turbulent motion. Hence, the relevant equations, for a so-called k-ε model, after lateral integration, are as follows:

Turbulent energy equation:

$$\frac{\partial(bk)}{\partial t}+\frac{\partial(buk)}{\partial x}+\frac{\partial(bwk)}{\partial z}$$
$$=bK_z\left(\frac{\partial u}{\partial z}\right)^2+\frac{\partial}{\partial z}\left(bK_{zk}\frac{\partial k}{\partial z}\right)$$
$$+\frac{\partial}{\partial x}\left(bK_{xk}\frac{\partial k}{\partial x}\right)+\frac{bgK_{zs}}{\rho_0}\frac{\partial \rho}{\partial z}-b\varepsilon \qquad (18)$$

Energy dissipation equation:

$$\frac{\partial(b\varepsilon)}{\partial t}+\frac{\partial(bu\varepsilon)}{\partial x}+\frac{\partial[bw\varepsilon]}{\partial z}$$
$$=c_1bK_z\frac{\varepsilon}{k}\left(\frac{\partial u}{\partial z}\right)^2+\frac{\partial}{\partial z}\left(bK_{z\varepsilon}\frac{\partial \varepsilon}{\partial z}\right)$$
$$+\frac{\partial}{\partial x}\left(bK_{x\varepsilon}\frac{\partial \varepsilon}{\partial x}\right)+\frac{c_2bgK_{zs}}{\rho_0}\frac{\partial \rho}{\partial z}-c_3b\varepsilon \qquad (19)$$

The energy dissipation process is associated with small-scale turbulence, so that it does not seem appropriate to use the dissipation equation here to determine the required turbulent length-scale l. Thus, Mellor and Yamada (1982) have proposed a turbulence model using directly the parameter pair k-l. Moreover, in equation (19), several coefficients have to be determined, and this is one of the main difficulties of the k- ε model. Therefore, the one-equation model (k equation) has been adopted here. But the rate of dissipation of k, in equation (19), must be expressed in terms of the mean properties of the turbulence field. Nihoul *et al.*, (1989) and Beckers (1991) define this expression as follows:

$$\left.\begin{aligned}&\varepsilon=\alpha_k\frac{k^2}{16K_z}\qquad \alpha_k\approx 1.0\\ &\text{with}\quad K_z=\frac{1}{2}\alpha_k^{1/4}\sqrt{kl_m};\qquad I_m=(1-R_f)I_{mo}(Z)\end{aligned}\right\} \qquad (20)$$

$$R_f=-\frac{K_{zs}}{K_z}R_i$$

with the Richardson number $$R_i\frac{g\frac{\partial \rho}{\partial z}}{\rho_0\left(\frac{\partial u}{\partial z}\right)^2} \qquad (21)$$

where R_f is the flux Richardson number and $l_{mo}(z)$ is the mixing length in the neutral case. The one-equation model is interesting as it considers the transport of the turbulent energy, but it is necessary to determine the mixing length. We used the formula proposed by Escudier (1966):

$$l_{mo}(z)=\min\left[K\alpha(\eta-z_f), K(z-z_f), K(\eta-z)\right] \qquad (22)$$

where η is the water surface elevation, z_f is the bottom elevation, K is the Karman constant (= 0.4) and α is a coefficient (= 0.19).

The boundary condition at the bottom, for equation (18) is as follows:

$$k|_{z=-h}\sim\frac{1}{\sqrt{C_\mu}}u_*^2 \qquad (23)$$

u_* is the friction velocity associated with the bottom friction stress, $u_*=(\tau/\rho)^{1/2}$.

Cμ is a constant (= 0.09, Rodi, 1980).

At the water surface, the turbulent energy is zero (no energy exchange between the water and the air).

At the downstream and upstream boundaries, the diffusive energy flux is equal to zero:

$$\frac{\partial k}{\partial x}=0 \qquad (24)$$

Coefficients of dispersion

Turbulent diffusion coefficients

K_{zs}, K_{zc} are calculated from Kz (Nihoul *et al.*, 1989):

$$\left.\begin{aligned}&K_{zs}\sim\gamma_s\sqrt{1-R_f}\;K_z\\ &K_{zc}\sim\gamma_c\sqrt{1-R_f}\;K_z\end{aligned}\right\} \qquad (25)$$

γ_s and γ_c are constant (=1.1).

Horizontal diffusion coefficients

Boerick and Hogan (1977) proposed an approximate relationship to calculate the momentum dispersion coefficient:

$$K_x=C_d\,b\,u \qquad (26)$$

where b is the width of the estuary and C_d a friction coefficient (= 0.0025).

The horizontal diffusion coefficients K_{xs} and K_{xc} are used as follows:

$$K_{xs} = K_x, \qquad K_{xc} = K_x \tag{27}$$

Coordinate transformation and numerical method

To take into account the real topography, a sigma transformation is adopted. Then, an arbitrary variable Φ is transformed as follows:

$$\Phi(x, z, t) \Rightarrow \Phi(x^*, \sigma, t^*)$$
$$\text{with} \quad x^* = x,\ t^* = t,\ \sigma = \frac{z+h}{\eta+h} = \frac{z+h}{H} \tag{28}$$

where h is the depth of the mean water level, η is the water elevation. σ ranges from zero at z = –h to one at z = η (Fig. 2). With this transformation, equations (1)-(4) and (18) become:

$$\frac{\partial(bu)}{\partial x^*} + \frac{\partial(bw^*)}{\partial \sigma} = 0 \tag{29}$$

$$\frac{\partial(bu)}{\partial t^*} + \frac{\partial(bu^2)}{\partial x^*} + \frac{\partial(buw^*)}{\partial \sigma}$$
$$= -bg\frac{\partial \eta}{\partial x^*} - b\alpha g H(1-\sigma)\frac{\partial S}{\partial x^*} - \frac{g}{Ch^2}u|u|\left(\left|\frac{\partial \chi}{\partial z}\right|_{y_1} + \left|\frac{\partial \chi}{\partial z}\right|_{y_2}\right)$$
$$+ \frac{\partial}{H^2 \partial \sigma}\left(bK_z\frac{\partial u}{\partial \sigma}\right) + \frac{\partial}{\partial x^*}\left(bK_x\frac{\partial u}{\partial x^*}\right) \tag{30}$$

$$\frac{\partial(bS)}{\partial t^*} + \frac{\partial(buS)}{\partial x^*} + \frac{\partial[bw^*S]}{\partial \sigma}$$
$$= \frac{\partial}{H^2 \partial \sigma}\left(bK_{zs}\frac{\partial S}{\partial \sigma}\right) + \frac{\partial}{\partial x^*}\left(bK_{xs}\frac{\partial S}{\partial x^*}\right) \tag{31}$$

$$\frac{\partial(bC)}{\partial t^*} + \frac{\partial(buC)}{\partial x^*} + \frac{\partial[b(w^* - w_s^*)C]}{\partial \sigma}$$
$$\frac{\partial}{H^2 \partial \sigma}\left(bK_{zc}\frac{\partial C}{\partial \sigma}\right) + \frac{\partial}{\partial x^*}\left(bK_{xc}\frac{\partial C}{\partial x^*}\right) \tag{32}$$

$$\frac{\partial(bk)}{\partial t^*} + \frac{\partial(buk)}{\partial x^*} + \frac{\partial[bw^*k]}{\partial \sigma}$$
$$= bK_z\left(\frac{\partial u}{H\partial \sigma}\right)^2 + \frac{\partial}{H^2 \partial \sigma}\left(bK_{zk}\frac{\partial k}{\partial \sigma}\right)$$
$$+ \frac{\partial}{\partial x^*}\left(bK_{xk}\frac{\partial k}{\partial x^*}\right) + \frac{bgK_{zs}}{\rho_0}\frac{\partial \rho}{H\partial \sigma} - b\varepsilon \tag{33}$$

The vertical "velocity" in the transformed system is:

$$w^* = -\frac{1}{H}\left[\sigma\frac{\partial \eta}{\partial t^*} + w\right] \tag{34}$$

The settling velocity is then:

$$w_s^* = \frac{w_s}{H} \tag{35}$$

The governing equations are solved by a splitting technique. The advection terms and the diffusion terms (including the wave propagation terms) are computed separately at each half-time step. The advection term is computed by the characteristic method and the diffusion term is computed with the finite difference method (Nguyen and Martin, 1988). Then, the second-order accurate central differences in space and the first-order forward differences in time are adopted. The scheme of the diffusion term is explicit regarding x and implicit regarding z, and is easily shown to be stable in this condition of calculation.

APPLICATION IN ACTUAL CONDITIONS

Physical parameters

The computation domain consists of three parts which correspond to the three branches of the estuary. The first branch is discretized in 35 sections with the longitudinal space step Δx = 2 km. The Garonne and Dordogne rivers, with two upstream ends: La Réole and Pessac, are respectively discretized in 24 and 25 sections, where Δx = 5 km. The vertical direction is discretized with 15 points which are refined near the bottom and the surface. For each point, the width b of the estuary is calculated by taking into account the water elevation (Fig. 4). The time step is Δt = 80 s.

The model operates with the tidal amplitude and river discharge values corresponding to the period of measurements made by the IGBA. (19-25 May, 1975). The measurements of current velocity, salinity and turbidity were obtained simultaneously, a fact which confers a major interest on this data set obtained 18 years ago. The tidal amplitude ranged between 2.8 and 3.6 m (tidal coefficient from 58 to 79) and the river discharges were about 450-480 $m^3.s^{-1}$ in the Garonne and 205-230 $m^3.s^{-1}$ in the Dordogne rivers respectively. The wind field during this period is unknown, so the shear stress τ_w at the water surface is set to zero in eq. 6. The numerical results are compared with those provided by IGBA at six stations located along six cross sections, from PK 20 to PK 75, close to the navigation channel. When matching calculated and measured values, the comparison is thus made between integrated values along the cross-section (calculated) and punctual values (measured). This may have no effect concerning the elevation values, because the water-surface slope regarding y can be neglected, but for the other parameters and mainly for the turbidity, comparison must be done with great care.

Sedimentological parameters

In this two-dimensional approach, the τ_{ce}, τ_{cd} and M parameters must take a unique mean value along each

cross-section. Thus, the values of these parameters, used by the model, are determined along the longitudinal axis (Fig. 6), taking into account a rough evaluation of the bed properties. For τ_{ce}:

– Regarding the sand bottom, extending from the estuary mouth to about 15 km upstream from Royan, and at the upstream boundaries, based on values reported by Hug (1975), τ_{ce} is proposed to be 2.0 ~ 3.0 N m^{-2}.

– Regarding the areas covered by the cohesive sediment, the τ_{ce} values are assumed to range from 0.5 to 1.7 N m^{-2} (Migniot, 1968). The T_{ce} value is set to 0.65 in the area where the fluid mud was located during the period of measurements. This area is established for the entire simulation.

The erosion constant M is also a knotty parameter to be determined. Cormault (1971) has proposed M to be equal to 2 10^{-3} kg m^{-2}.s^{-1}, based on laboratory measurements using a composite mud of the Gironde estuary. In the model, M varies from 2 10^{-3} to 3 10^{-2} kg m^{-2}.s^{-1}. The highest value ascribed to M corresponds to the softest mud having the lowest τ_{ce} values, *i.e.* where the fluid mud is located.

The state of consolidation of the sediment along the estuary varies with time, strongly with seasonal river flow and probably with tidal amplitude. These variations may induce some fluctuations of the bed shear strength values and thus of the τ_{ce} and M values. But, in this first approach, for a simulation of a few days period, these parameters are considered constants. This also means that the freshly-deposited matter obtains instantaneously the τ_{ce} and M values assumed to be in its sedimentation location (Le Hir and Karlikow, 1991). The quantities of sediment and fluid mud available for the erosion process are considered limitless.

The τ_{cd} value, below which deposition occurs, is principally characterized by the nature and the concentration of the suspended matter and has been measured in many laboratory experiments: for the San Francisco bay, with sediment having uniform properties, Krone (1962) found τ_{cd} = 0.078 N m^{-2} when the initial TSM ranged from 0.3 to 10 g.l^{-1}; for sediment having a broad size distribution, Mehta and Partheniades (1975) found that τ_{cd} varies from 0.18 N m^{-2} to 1.1 N m^{-2}. However, there are few laboratory studies using the mud of the Gironde. Based on the variation of the minimum value of the calculated bottom shear stress calculated by the model, τ_{cd} is set to 0.3 ~ 0.5 N m^{-2}.

Upstream from PK 20, there is no turbidity maximum influence during the considered period of measurements; the TSM concentration is very low. Thus, the figures showing the calculated results cover the area from PK 20 to the mouth of the estuary.

Initial conditions

The computational time needed to obtain a stable periodic solution can be reduced by using some selected initial values.

The computation starts at a time corresponding to slack water. The initial values for the surface elevation are set to 1.4 m at each section. The initial velocity distribution is u = 0.1 ms^{-1} and w = 0.0015 m.s^{-1}. The initial salinity is obtained by a linear interpolation between the values at the top and the bottom of the water column. The concentration of TSM is set to 0.1 g.l^{-1} for the Gironde estuary and to 0.05 g.l^{-1} for the rivers. With these initial conditions, after two tidal periods of calculation, the stable periodic regime is reached.

RESULTS AND DISCUSSION

The tidal time indicated in the figures is referred to that at the mouth (Pointe de Grave). The origin time in the figures representing the results is delayed by three tidal periods from the starting time of the simulation.

Estuarine circulation

The surface elevation is continuously recorded along the Gironde estuary: this surface is very well described by the model (Fig. 7). The differences between the corresponding computed and measured values are less than 2% in amplitude and less than 10 minutes in phase. Moreover, the

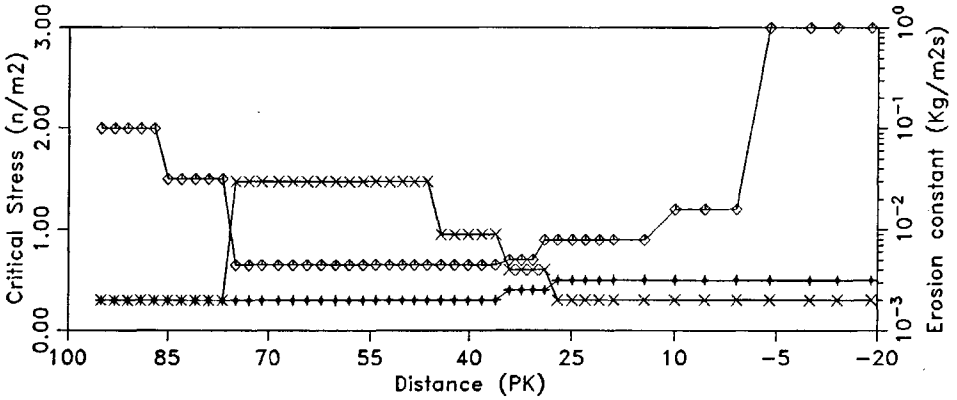

Figure 6

Longitudinal distribution of the critical bottom shear stresses and the erosion constant values used during the considered period of the simulation.

numerical results show clearly that the tidal amplitude increases landward from the mouth of the estuary. This is in agreement with the fact that the Gironde is a hypersynchroneous estuary (Salomon and Allen, 1983).

Longitudinal current velocities one metre below the surface and one metre above the bottom are shown in Figure 8. The phase difference between the numerical results and the observed ones is less than 5 minutes. The computed values of the current velocity are fairly in agreement with the observed ones (differences smaller than 15%). However, at Richard, during the tidal flow, the numerical value of the maximum velocity is higher than the observed ones; but Richard is located 20 km upstream, from the mouth, where the depth of the estuary varies rapidly and where the transverse component of the horizontal circulation exists. The instantaneous velocity field every 2 hours during one tidal cycle (tidal coefficient 75 ~79) is illustrated in Figure 9.

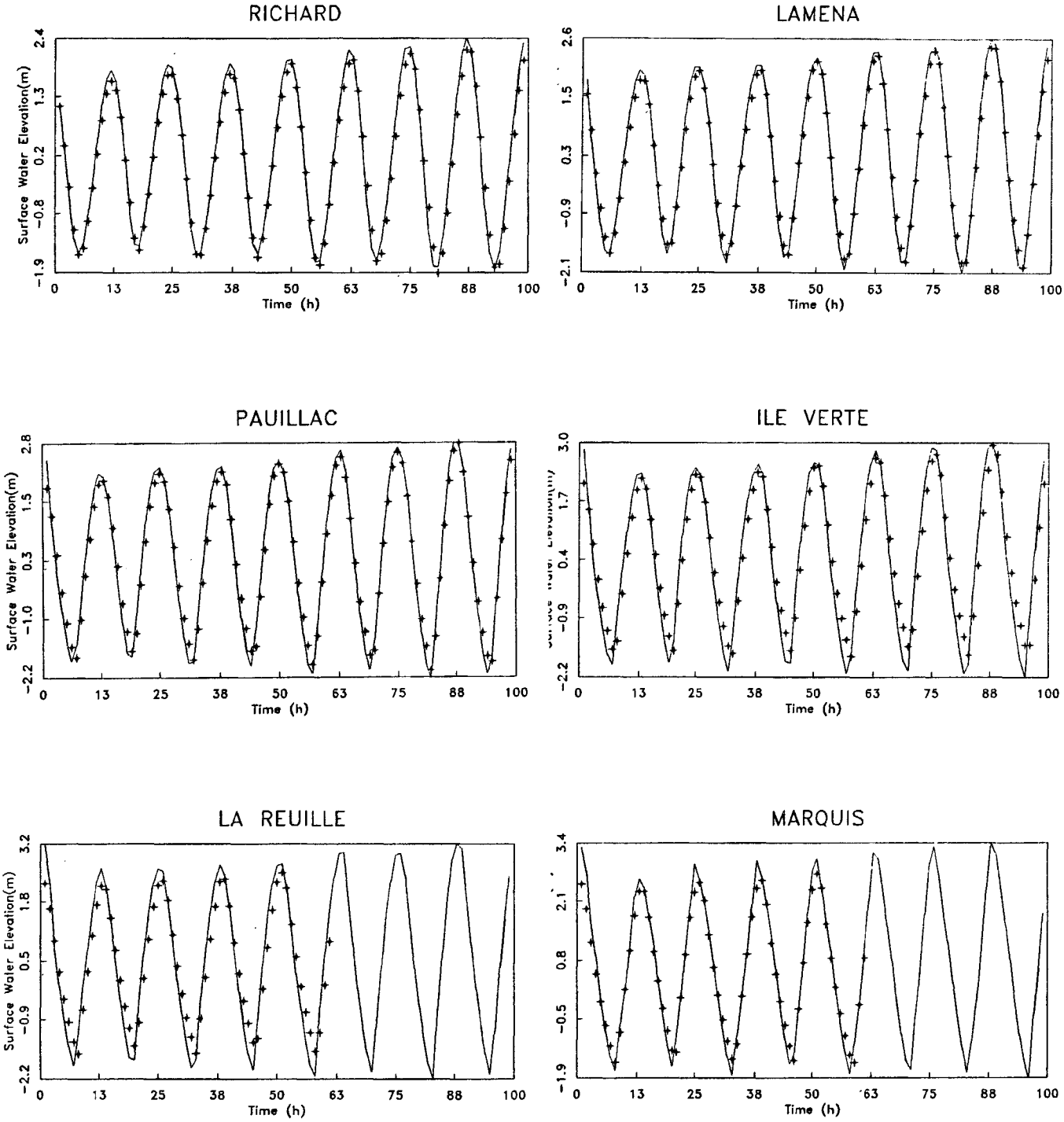

Figure 7

Comparison of observed (cross) and computed (continous lines) elevations at 6 locations (tidal amplitude from 2.8 to 3.6 m, mean river discharge ≈ 700 $m^3.s^{-1}$).

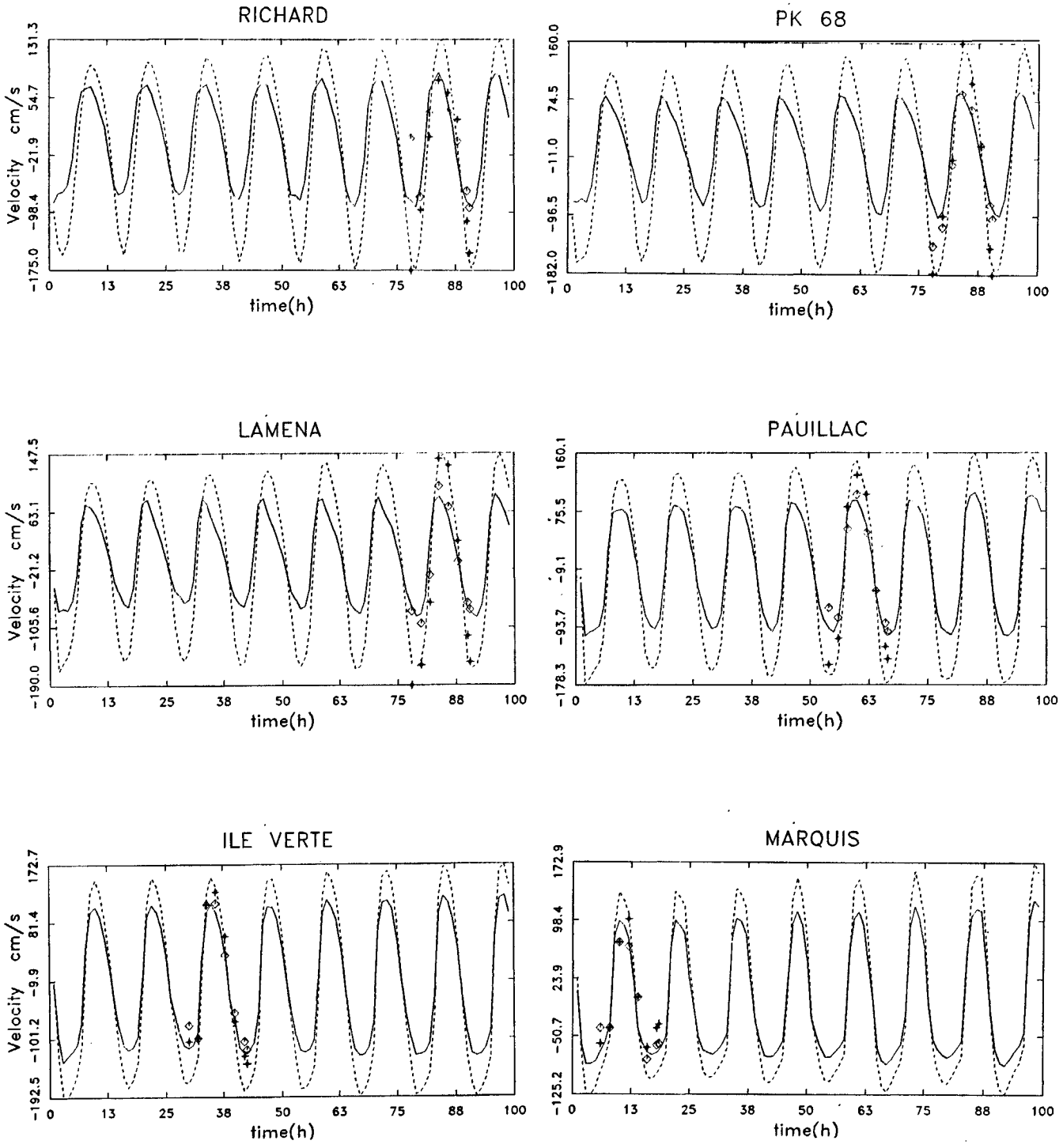

Figure 8

Comparaison of computed and observed velocity at 1 m below the surface and 1 m above the bottom (tidal amplitude from 2.8 to 3.6 m, mean river discharge = 700 $m^3.s^{-1}$).

The turbulent energy field permits a detailed illustration of the influence of tidal effects. Turbulent energy distribution every 2 hours during one tidal cycle is shown in Figure 10. The energy is always higher close to the bottom than to the surface (the wind effect is ignored). The field reaches its peak between high tide plus 4 hours and low tide, and the maximum value at the bottom can .exceed 5 10^{-3} $m^2.s^{-2}$ (Fig.10*f*, *a*). It presents a uniform state with the lowest values at high tide plus 2 hours and at low tide plus 2 hours (Fig.10*b*,*e*). A simple relationship between the turbulent energy field and the current velocity field is not obvious (Fig. 8 and 9); except when the current velocity is very low, the turbulent energy is also very weak.

Calculated salinity values *versus* the measured ones are shown (Fig.11). The lag time between them is less than

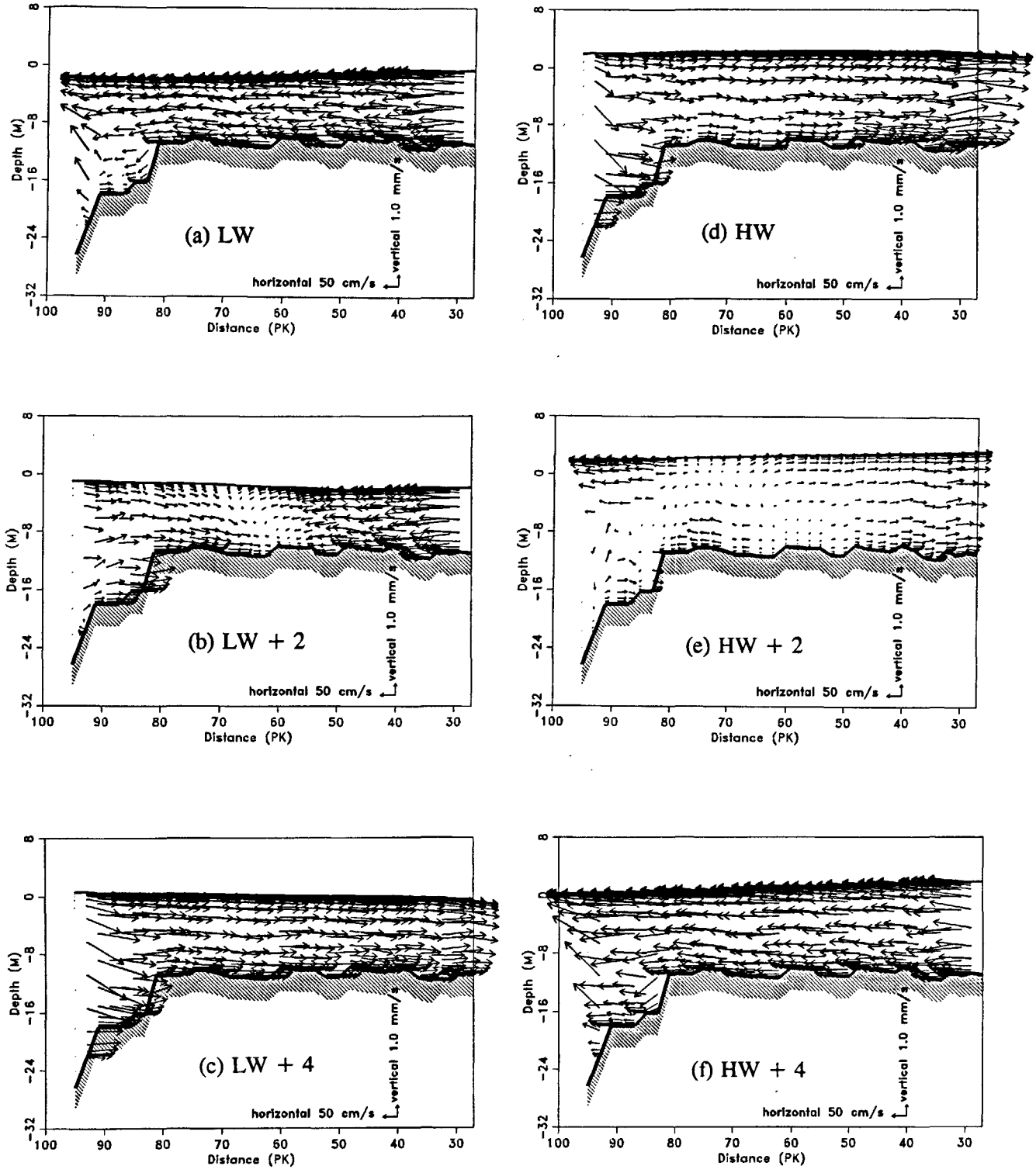

Figure 9

Instantaneous velocity field during one tidal cycle (tidal amplitude ≈ 3.5 m, mean river discharge ≈ 700 $m^3.s^{-1}$).

20 minutes. The decrease in mean salinity from 30 $g.l^{-1}$ at the mouth to 1 $g.l^{-1}$ at Marquis is well shown. The calculated salinity values fit well the measured data, regarding the tide phase, upstream from Lamena (differences < 20%). Downstream from Lamena (Richard and PK 68), salinity values at the water surface are smaller than the observed ones. This could indicate that the computed vertical salinity mixing is not strong enough despite the noticeable advantage induced by the turbulence closure sub-model used here; or it could be due to the limitations of the two-dimensional vertical model in this area, where a transverse horizontal circulation exists. The process of the salinity intrusion is also shown by the salinity distribution (Fig.12). Two hours after low tide, the isohaline 1 $g.l^{-1}$ reaches PK 40 (Fig.12 *b*). Two hours after high tide, it is located upstream of PK 30 (Fig.12 *e*). This means that a displacement of more than 10 km in the salinity pattern occurs during one semi-tidal cycle.

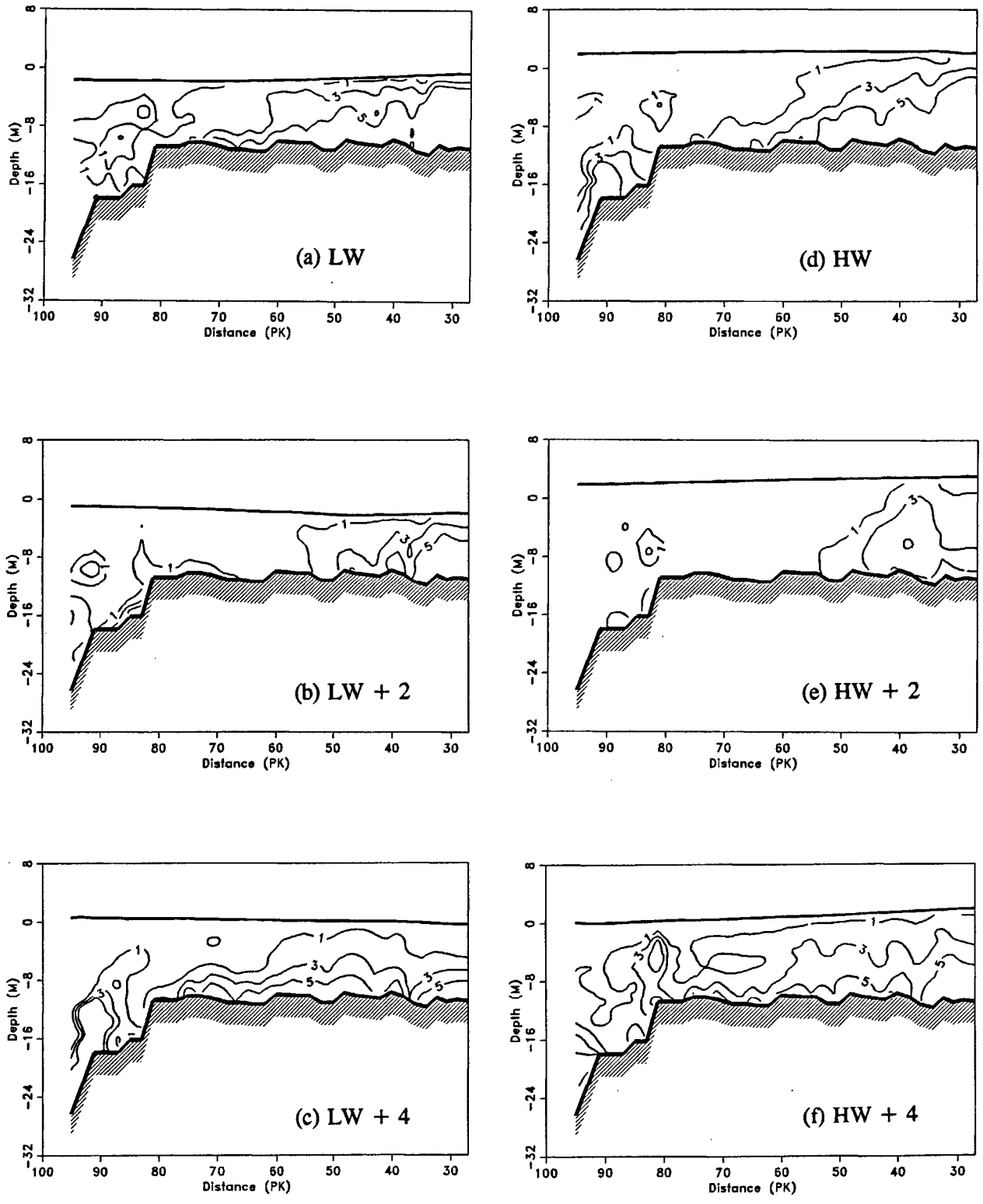

Figure 10

Distribution of the turbulent energy (10^{-3} $m^2.s^{-2}$) during one tidal cycle (tidal amplitude ≈ 3.5 m, mean river discharge ≈ 700 $m^3.s^{-1}$).

Turbidity

The complexity of the physics of the natural Gironde estuarine environment, principally the variability of the bed properties (τ_{ce} and M) along a cross-section and the limitation of a two-dimensional vertical model, do not allow a full calibration of the model. For each section of the estuary, a mean value, for τ_{ce} and for the M parameters, is considered, taking into account our knowledge of these parameters in the natural environment (see section Sedimentological Parameters). Thus, two tests were performed.

– First, a unique value for τ_{ce} (1.2 $N.m^{-2}$) and M (6 10^{-3} $kg.m^{-2}.s^{-1}$) was set from PK 10 to PK 80, in order to verify whether the simulated turbidity maximum location does not depend solely on the τ_{ce} and M values assumed in the area where the fluid mud exists. For these

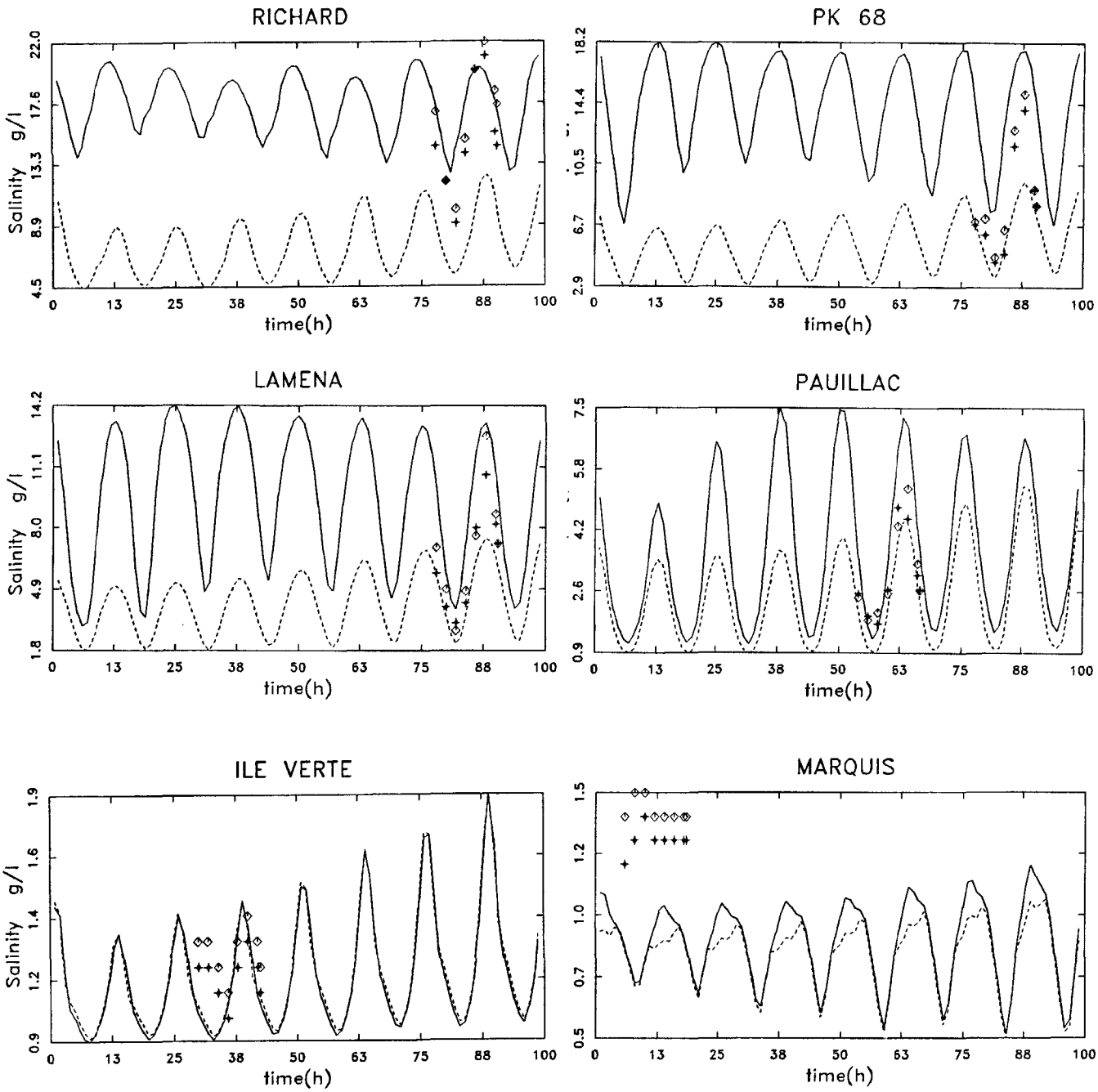

Figure 11

Comparaison of computed and observed salinity at 1 m below the surface and 1 m above the bottom (tidal amplitude from 2.8 to 3.6 m, mean river discharge ≈ 700 $m^3.s^{-1}$).

conditions, the location of the turbidity maximum is the same as that described hereafter, but its intensity is much less than the observed one.

– Second, a sensibility test was performed to show how the simulation of the turbidity maximum is affected by the change of the assumed τ_{ce} and M values, in the area where the fluid mud occurs. The test is based on the effects of these changes on the calculation of the total mass of the turbidity maximum, by reference to the mass obtained with the assumed parameters. This, for a 5-day period simulation, with a constant tidal amplitude of 3.35 metres (tidal coefficient of 70). When the assumed value of M is multiplied by 10, the total mass of the turbidity maximum increases by 30%; when this value is divided by 10, the mass decreases by 13%. When the assumed value of τ_{ce} is increased by 30%, the total mass of the turbidity maximum decreases by 13%; when this value is decreased by 30%, the total mass increases by 43%. This test shows that the model is not too greatly affected by some uncertainties concerning the τ_{ce} and M parameter values.

The main characteristics of the turbidity maximum, its formation and decay and its displacement during one tidal

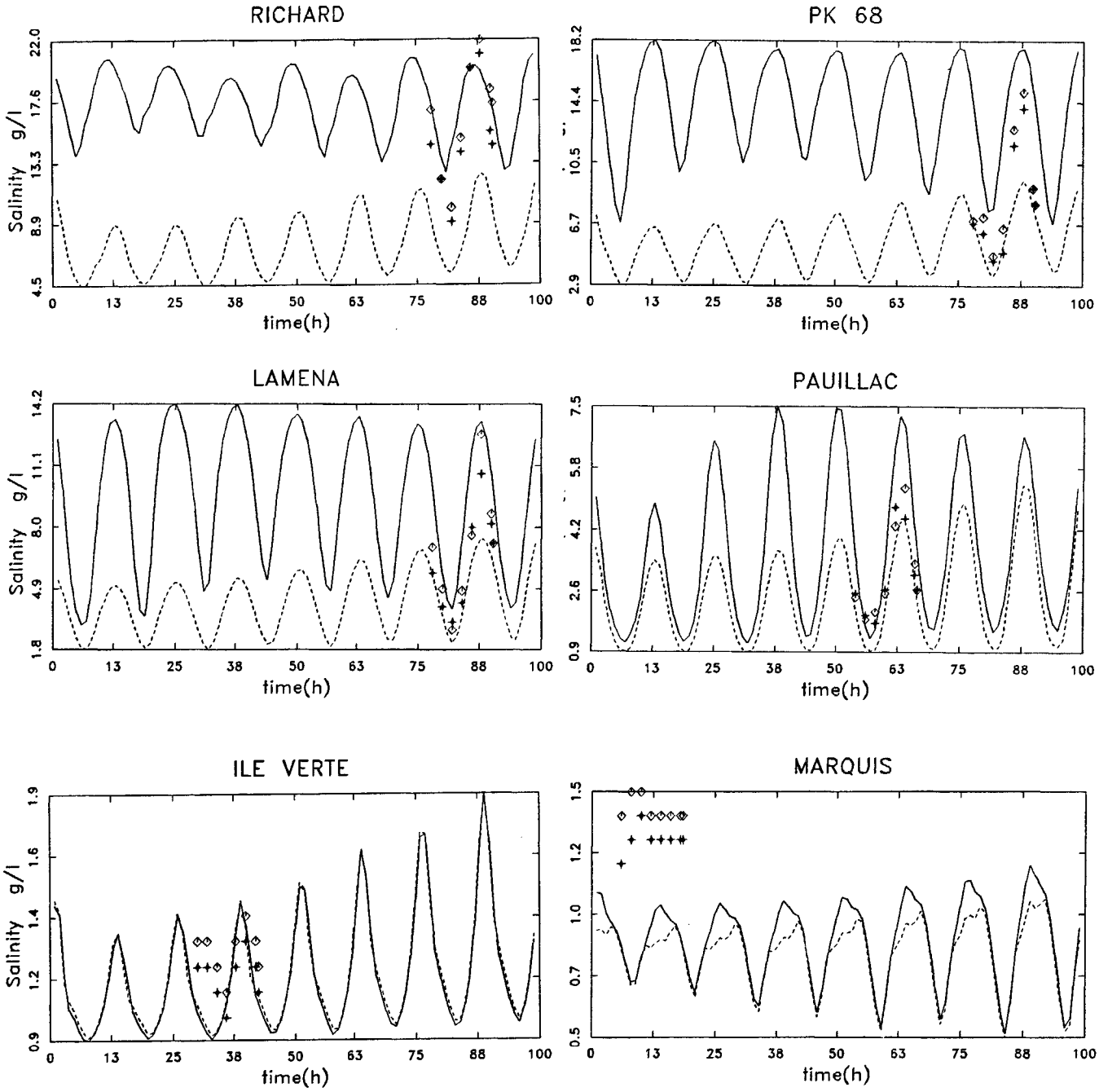

Figure 12

Longitudinal distribution of salinity (‰) during one tidal cycle (tidal amplitude ≈ 3.5 m, mean river discharge ≈ 700 $m^3.s^{-1}$).

cycle for the tidal amplitudes and the river discharge corresponding to the period of measurements are shown.

The time evolution of the calculated turbidity (Fig.13) shows that the TSM concentration increases during the portion of the 5 days corresponding to the increase of the tidal coefficient greater than 60. The computed TSM values are in good agreement with the observed data. The observed maximum of the TSM concentration, at Lamena, is also shown by the model, despite the fact that the calculated bottom turbidity value is less than the observed one.

Turbidity one metre above the bottom shows (clearly from Pauillac to the estuary mouth) two maximum values during one tidal cycle. This is related to the module of bottom current velocity which displays two maxima during one tidal cycle.

At Richard, the TSM concentration is greater during the ebb than during the flood, while the bottom current velocity is symmetrical during one tidal cycle. Richard is located at the seaward end of the turbidity maximum zone; consequently, due to the dilution resulting from the sea water intrusion during the flood, the TSM concentration is lower during this period. On the contrary, at Marquis located upstream the turbidity maximum, the greatest TSM concentration appears during the flood.

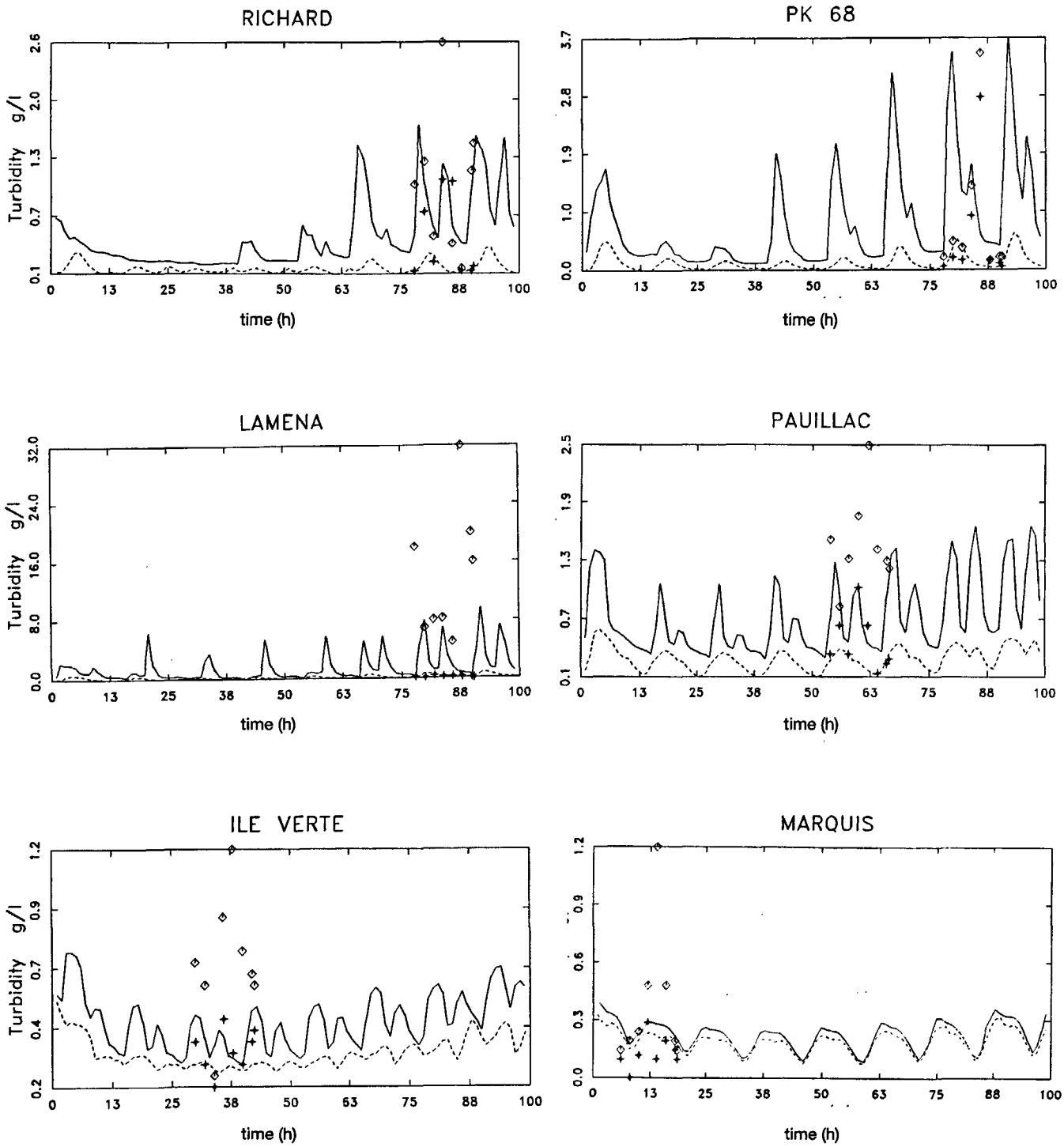

Figure 13

Comparaison of computed and observed turbidity at 1 m below the surface and 1 m above the bottom (tidal amplitude from 2.8 to 3.6 m, mean river discharge ≈ 700 m^3s^{-1}).

The evolution of the turbidity maximum every 2 hours during one tidal cycle is represented Figure 14. The turbidity maximum zone with a concentration > 1 $g.l^{-1}$ spreads over about 40 km; its core (> 5$g.l^{-1}$) is situated at PK 65 at low tide (Fig.14 *a*). It has a longitudinal oscillation of 15 km during one tidal cycle: at high tide, the seaward boundary of the maximum is displaced upstream, and its core is situated at PK 50 (Fig.14 *d*). The size and the intensity of the maximum strongly depends on the phase of the tide cycle: after low and high tide, its concentration decreases (Fig.14 *b*, *e*). Conversely, with the increase of current velocity, the maximum arises again (Fig.14 *c*, *f*).

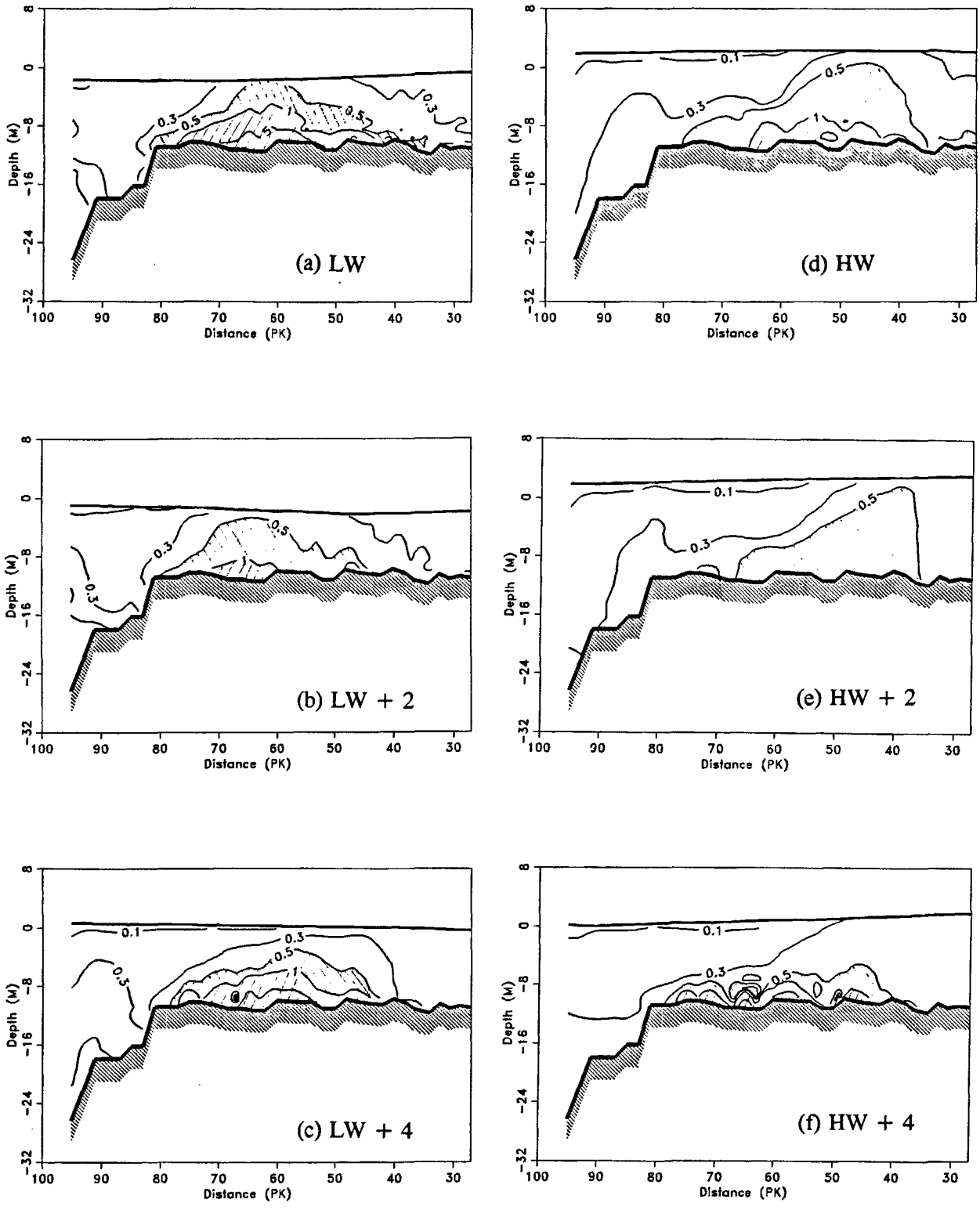

Figure 14

Evolution of the "turbidity maximum" ($g.l^{-1}$) during one total cycle (tidal amplitude ≈ 3.5m, mean river discharge ≈ 700 $m^3.s^{-1}$).

The use of a turbulence closure sub-model induces several effects on the turbulent viscosity and diffusion coefficient values. Thus, compared with the use of the mixing-length method, the calculated turbidity maximum seems to match better the observed structure (Fig.15).

The simulated results are also compared with the scheme of the longitudinal turbidity distribution given by Castaing (1981) (Fig.16). The observed values were collected in the navigation channel on 22 May, 1974 with a spring tidal amplitude of 4.1 m (tidal coefficient of 91-93) and a mean river discharge of 600 $m^3.s^{-1}$. The simulated results are in

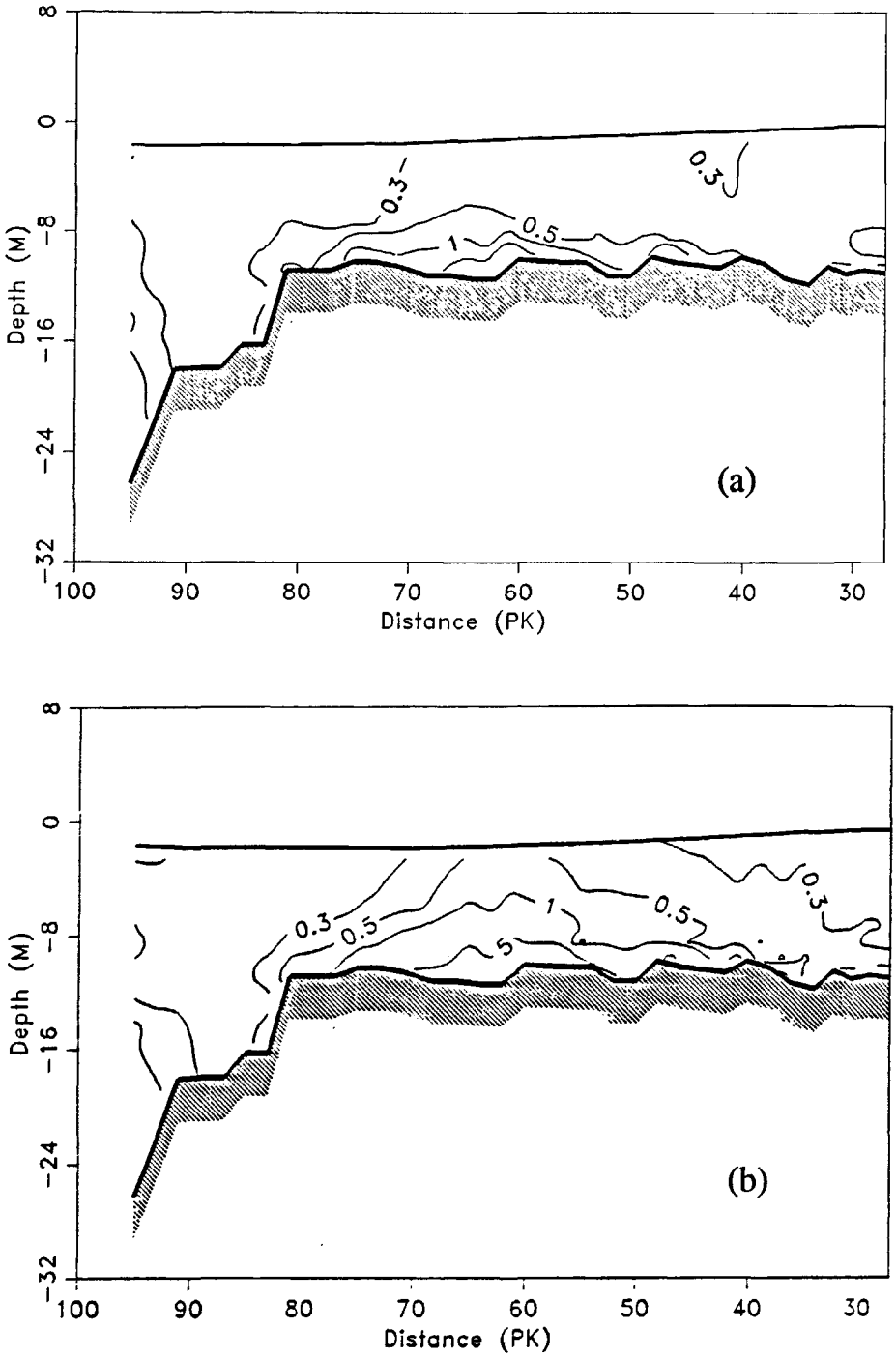

Figure 15

"Turbidity maximum" at Low Tide calculated with different turbulence models: a) mixing length model; b) one equation model.

good agreement with the turbidity pattern reconstructed by Castaing, especially the decay of the TSM intensity two hours after high tide (Fig.16 *d*).

The calculated total mass of the TSM in the estuary has its maximum value (2 10^6 T) at high tide and its minimum value (1.3 10^6 T) at low tide. The mean total mass of TSM deduced from the *in situ* results during a spring tide (Allen, 1973) falls close to 2.5 10^6 T.

The tidal amplitudes 2.5 m and 4.1 m (tidal coefficient of 50 and 90) which are outside the observed ones are also used to examine the response of the model, with a constant water discharge of 700 $m^3.s^{-1}$. The tidal coefficient 90 induces an increase of the intensity of the turbidity maximum, the total mass of the TSM is 2.2 10^6 T and a fraction of the maximum is flushed towards the sea (Fig.17) at low tide. For a tidal coefficient of 50, there is a large decrease of the size and of the intensity of the maximum (Fig.18). The total mass of the TSM is 0.45 10^6 T and there is practically no flux of TSM towards the sea. These effects of low and high tidal amplitude have indeed been observed (Allen, 1973 and Castaing, 1981).

In this model, the TSM settling velocity is only a function of the TSM concentration, following the Thorn (1981) results. This means that particle size distribution is not taken into account, in spite of its dramatic change in the low salinity zone, depending on the flocculation process. An improvement of this model implies that account must be taken of particle size distribution, bed shear strength which depends of the state of the sediment consolidation, and finally of the history, on short and long time scales, of the estuary.

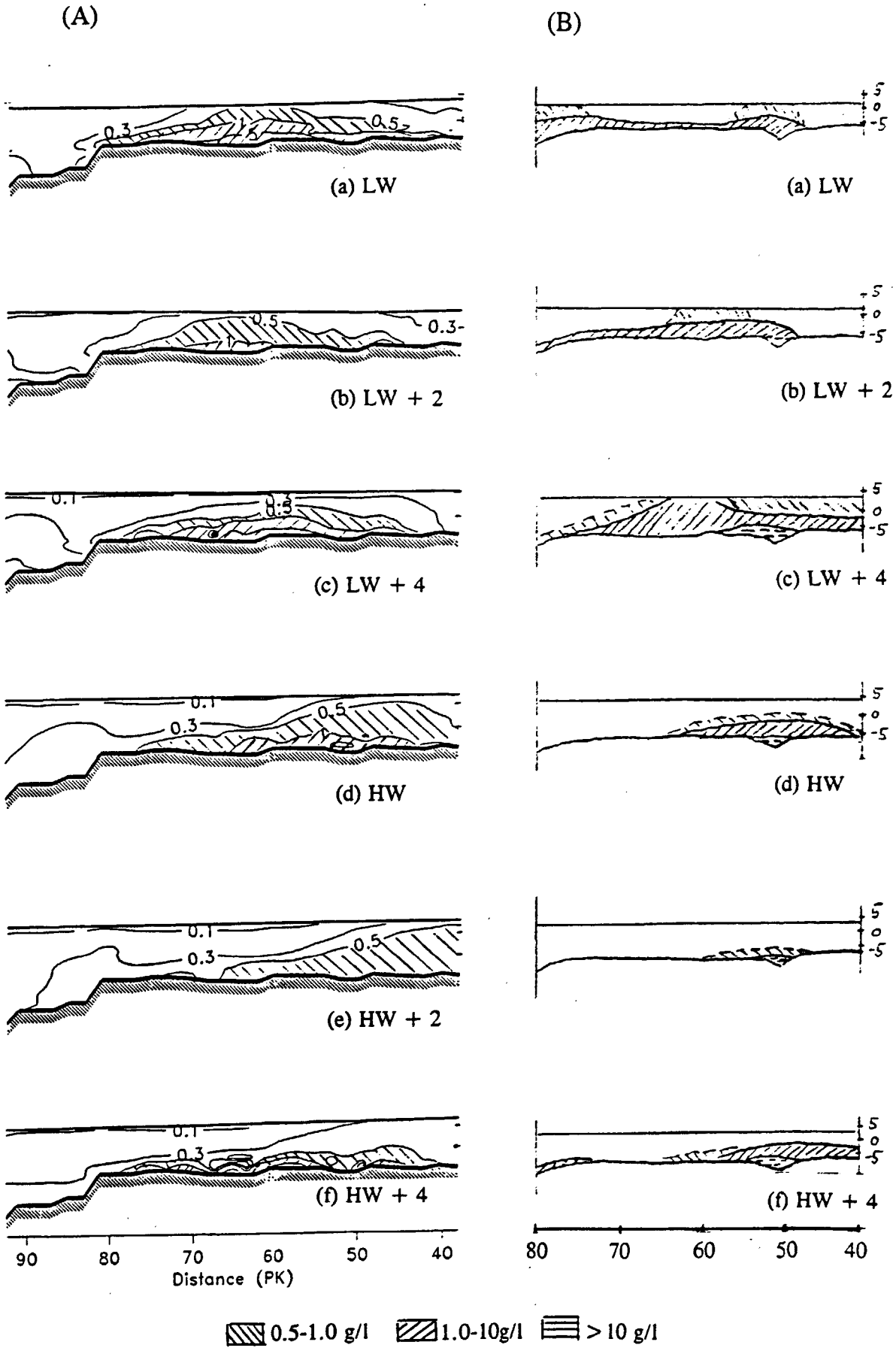

Figure 16

Comparaison of the numerical turbidity distribution ($g.l^{-1}$) (A) and the observed distribution (B) (Castaing, 1981) during a spring tidal cycle (tidal amplitude ≈ 4.1 m, mean river discharge ≈ 700 $m^3.s^{-1}$).

CONCLUSION

A vertical two-dimensional width-integrated model, coupled with a turbulence closure sub-model, has been used to simulate the estuarine circulation, the salinity intrusion and the total suspended matter transport process in the Gironde estuary. The detailed time evolutions of the elevation, the velocity, the salinity and the turbidity during five days with a tidal amplitude varying from 2.8 to 3.6 m, have been calculated and compared with the observed data at six stations along the estuary axis. The longitudinal distributions of salinity, turbidity and turbulent energy during one tidal cycle have been described to illustrate the semi-diurnal tidal effects on these processes in this macrotidal estuary.

The results indicate that:

a) The computed hydrodynamical variables are in good agreement with the observed data.

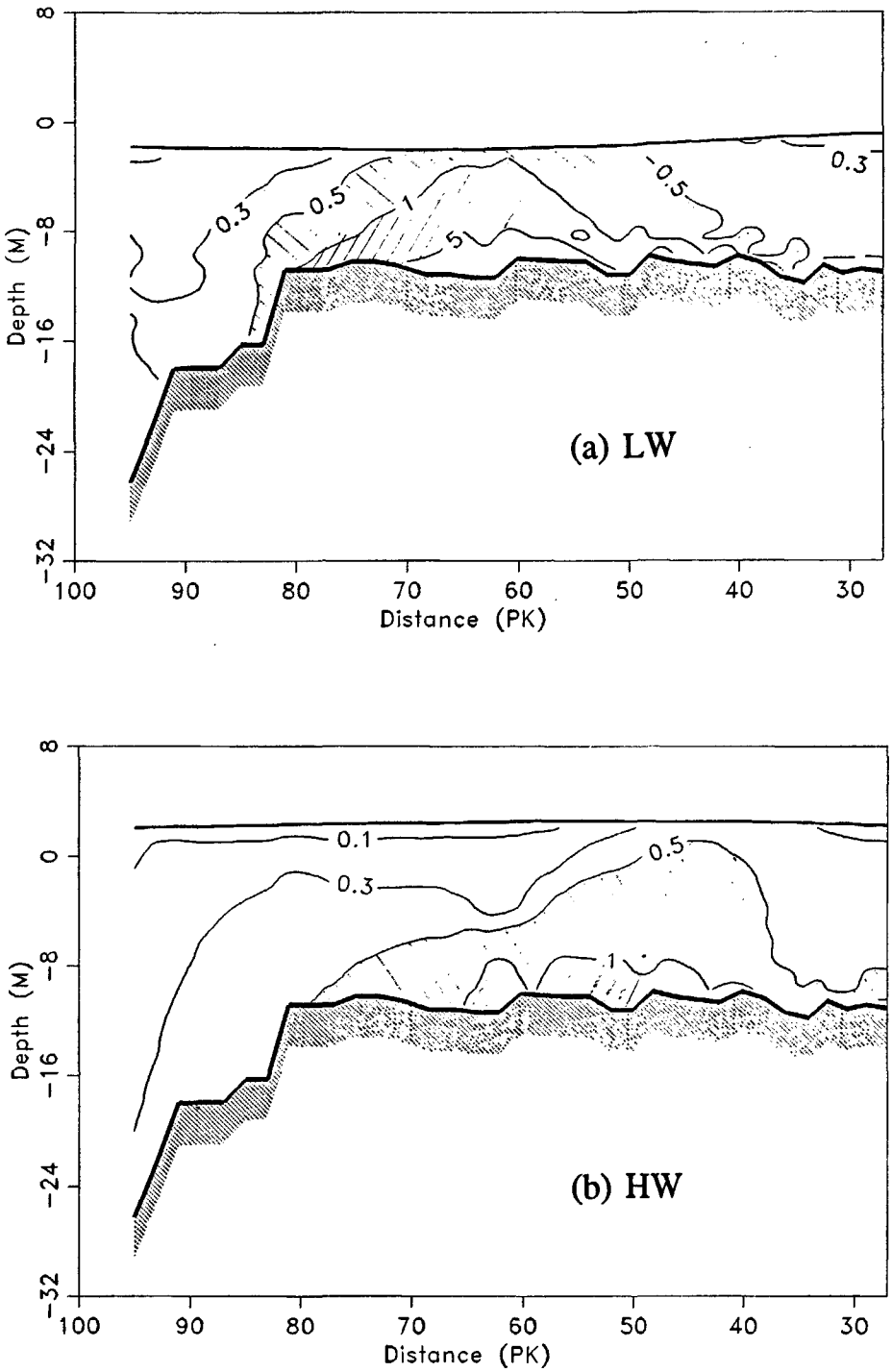

Figure 17

Displacement of the "turbidity maximum" ($g.l^{-1}$) during a spring tidal cycle (tidal amplitude ≈ 4.1 m, mean river discharge ≈ 700 $m^3.s^{-1}$)

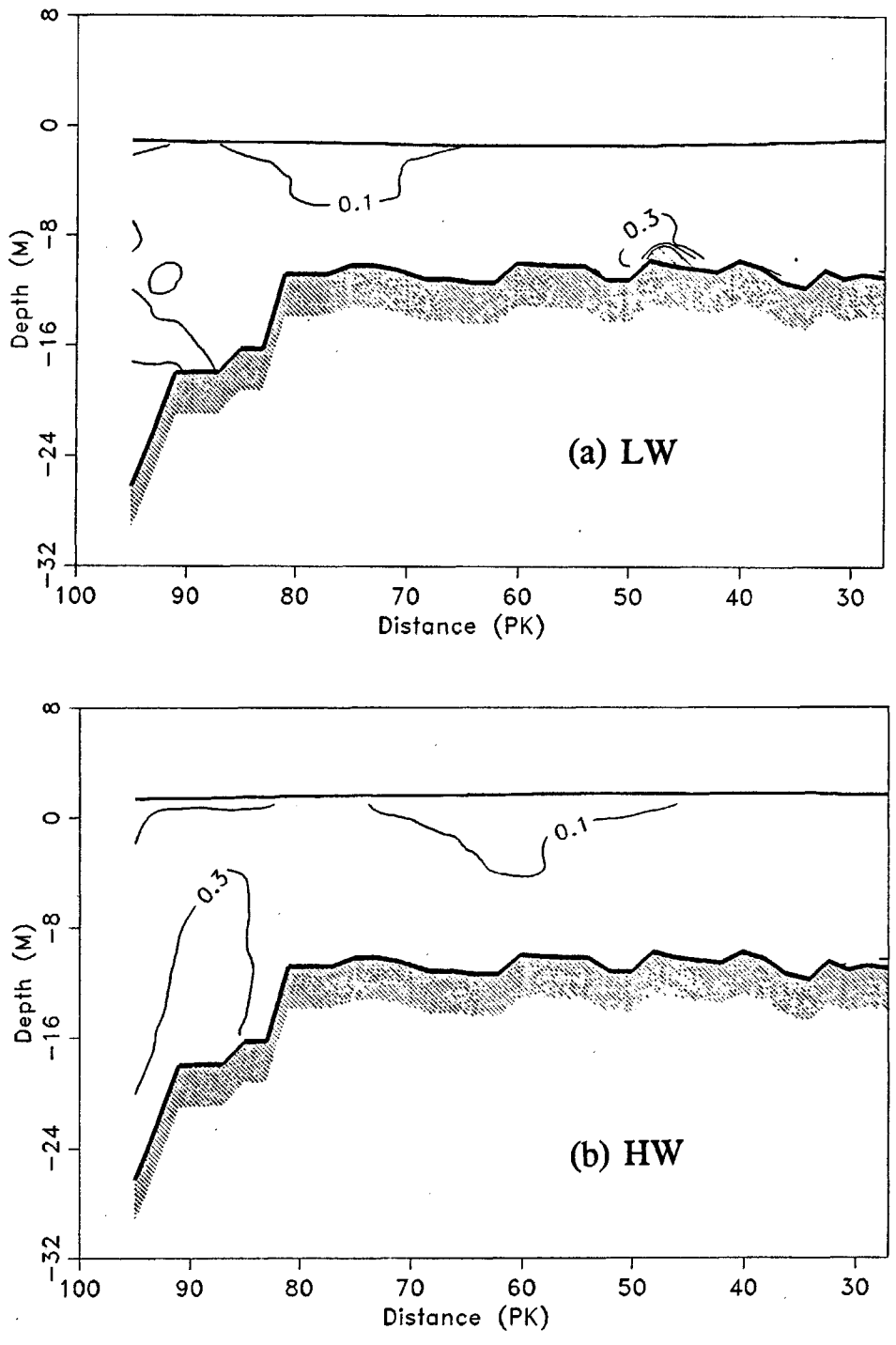

Figure 18

Displacement of the "turbidity maximum" ($g.l^{-1}$) during a neap tidal cycle (tidal amplitude ≈ 2.5 m, mean river discharge ≈ 700 $m^3.s^{-1}$)

b) The tidal oscillation induces a 15 km displacement of the turbidity maximum during one tidal cycle. The formation and the decay of this maximum have been simulated, and the total mass of the maximum obtained by the model is in good agreement with the observed one. Turbidity maximum behaviour is strongly controlled by the turbulent energy field, connected with the macrotidal mechanisms.

c) An increase of the tidal amplitude up to 4.1 m, provokes the increase of the size and the intensity of the turbidity maximum and its partial flushing to the sea.

Acknowledgements

We acknowledge support from the Commission of the European Communities under contract MAST 0024C.

The authors are also gratefull to Prof. J.C.J. Nihoul and Dr. J.M. Beckers for improving the description of turbulence in the model. We also thank Mr. W.Y. Xu and Mr L.X. Dong for their initial contribution to the project and Dr. P. Le Hir for his helpful comments.

REFERENCES

Allen G.P. (1973). Etude des processus sédimentaires dans l'estuaire de la Gironde. Thèse Doct. Sci. Nat. Bordeaux. 314 p.

ASCE (1988). Turbulence modeling of surface water flow and transport. *J. Hyd. Eng.*, Part. 1, Vol. 114, 9, Sept., 970-991.

Baumgartnen M. (1836-1844) unpublished, quoted by Levèque F. (1936).

Beckers J.M. (1991) Application of the GHER 3D general circulation model to the Western Mediterranean, *J. Marine Systems.*, **1**, 315-332.

Blumberg A.F. and G.L. Mellor (1987). A description of a three-dimensional coastal ocean circulation model, Three-dimensional coastal ocean models, *Coastal and Estuarine Sciences*, 1-16.

Boerick R.R. and J.M. Hogan (1977). An x-z hydraulic/thermal model for estuaries, Hyd. Div., ASCE, **103**, 19-37.

Bradshaw P. (1978). Turbulence. Topics in Applied Phys., Vol 12.

Castaing P. (1981). Le transfert à l'océan des suspensions estuariennes (cas de la Gironde). Thèse Doct. Sci. Nat. Bordeaux. 530 p.

Cormault P. (1971). Détermination expérimentale du débit solide d'érosion de sédiments fins cohésifs. 14e Congrès Assoc. Int. Rech. Hydraul., Paris, 29 août-3 septembre 1971, t.4, 2-8.

Dyer K.R. (1988). Fine sediment particle transport in estuaries. Physical Processes in Estuaries, edited by J. Dronkers and W. van Leussen, 295-310.

Dyer K.R. (1986). Coastal and Estuarine Sediment Dynamics. John Wiley & Sons. Chichester. 342 p.

Du Penhoat Y. and J.C. Salomon (1979). Simulation numérique du « bouchon vaseux » en estuaire, Application à la Gironde. *Oceanol. Acta.*, **2**, (3), 253-260.

Einstein H.A. and R.B. Krone (1962). Experiments to determine modes of cohesive sediment transport in salt water, *J. G. Res.*, **67**, No.4, April.

Eisma D., P. Bernard, G.C. Cadée, V. Ittekkot., J. Kalf, R. Laane, J.M. Martin, W.G. Mook, A. Van Put and T. Schuhmacher (1991). Suspended-matter particle size in some west-european estuaries. *Neth. J.Sea Res.*, **28** (3), 193-214.

Escudier M.P. (1966). The distribution of mixing-length in turbulent flow near walls, Imperial College, Heat transfert Section, Report TWF/TN/1.

Falconer R. and P. Owens. (1991). Numerical modelling of suspended sediment fluxes in estuarine waters. *Estuar. Coast. Shelf Sci.*, **31** (6), p 745-762.

Galperin B. and G. L. Mellor (1990) A Time-dependent, Three-dimensional Model of the Delaware Bay and River System, *Estuar. Coast. Shelf Sci.*, **31**, 231-253.

Glangeaud L. (1939). Le rôle de la suspension tourbillonnaire et de la traction sur le fond dans la formation des sédiments de la Gironde. *C.R. Acad.Sci. Paris*, 208, p. 1595

Hamilton P. (1975). A numerical model of vertical circulation of tidal estuaries and its application to the Rotterdam Waterway. *Geophys. J.R.Astron. Soc.*, **40**, 1-21

Hug M. (1975). Mécanique des fluides appliquée, ed. Eyrolles, Paris 1185 p.

I.G.B.A. (1975). Mesure de vitesse, salinité et concentration en Gironde et Garonne. Mai. (cadre des études EDF), 43 p.

Inglis C.C. and F.H. Allen (1957). The regime of the Thames estuary as affected by currents, salinities and river flow. *Proc. Inst. Civ. Engin.*, **7**, 827-868.

Jouanneau J.M. and C. Latouche (1981). The Gironde Estuary, edited by H. Fuchtbauer, A.P. Lisitzyn, J.D. Milliman and E. Seibold. 115 p.

Krone R.B. (1962). Flume studies of the transport of sediment in estuarial processes. Final Report, *Hydrau. Eng. Lab. and Sanitary Eng. Res. Lab.*, Univ. of California, Berkeley, Calif.

Le Hir P. and N. Karlikow (1991). Balance between Turbidity Maximum and Fluid Mud in the Loire estuary. Lessons of a first mathematical modelling. Int. Symp. The transport of suspended sediment and its mathematical modelling. Florence (Italy), Sept. 2-5,1991, 449-466.

Levèque F. (1936). Bordeaux et l'estuaire girondin. Imprimerie Delmas, Bordeaux, 167 pp.

Martin J.M., J.M. Mouchel and A.J. Thomas (1986). Time concepts in hydrodynamic systems with an application to ^{7}Be in the Gironde estuary. *Mar. Chem.*, **18**, 369-392.

Mehta A.J. and E. Partheniades (1975). An investigation of the depositional properties of flocculated fine sediments. *J. Hydr. Res.*, **12**(4), 361-609.

Mehta A.J. (1986). Characterization of cohesive sediment properties and transport processes in estuaries. Estuarine Cohesive Sediment Dynamics, edited by A. J. Mehta, Springer-Verlag, New York, 290-325.

Mehta A.J. (1988). Laboratory studies on cohesive sediment deposition and erosion. Physical Processes in Estuaries, edited by J. Dronkers and W. van Leussen, 427-445.

Migniot C. (1968). Etudes des propriétés physiques de différents sédiments très fins et de leur comportement sous des actions hydrodynamiques. *Houille Blanche*, **7**, 591-620.

Migniot C. (1971). L'évolution de la Gironde au cours des temps. *Bull. Inst. Géol. Bassin Aquitaine* **11**, 221-281.

Mellor G.L. and T. Yamada (1982) Development of a turbulence closure model for geophysical fluid problems. *Reviews of Geophysics and Space Physics*, **20**, 851-875.

Nguyen K.D. and J.M. Martin (1988). A two-dimensional fourth order simulation for scalar transport in estuaries and coastal seas, *Estuar. Coast. Shelf Sci.*, **27**, 263-281.

Nguyen K.D. (1987). Modélisation numérique 2-D et 3-D de la circulation générale en milieu estuarien èt côtier. Thèse. Université P. et M. Curie, Paris, 99 p.

Nihoul J.C.J., E. Deleersnijder and S. Djenidi (1989). Modelling the general circulation of shelf seas by 3-D K-ε models, *Earth Sciences Reviews*, **26**, 163-189.

Odd N.V.M and M.W. Owen (1972). A two-layer model of mud transport in the Thames estuary. Proceedings ICE Paper 7517S, 175-205.

Parthenaides E. (1962). A study of erosion and deposition of cohesive soils in salt water. Ph.D Thesis. University of California, Berkeley, 182 p.

Ramette M. (1981). Guide de l'hydraulique fluviale. Rapport interne HE 40/81.04, Electricité de France.

Rodger J.G. and N.V.M. Odd (1985). A mathematical model of mud transport in deep partially mixed canalized estuaries. *Hydraul. Res. Rep.*, SR:37.

Rodi W. (1980). Turbulence models and their application in hydraulics, Monograph, International Association for Hydraulic Research, Delft, The Netherlands. 648 p.

Salomon J.C. and G.P. Allen (1983). Rôle sédimentologique de la marée dans les estuaires à fort marnage. Cie Fr.Pétr. Notes Mém.,**18**, 35-44.

Sauvaget, P. (1987). Modélisation numérique des écoulements stratifiés en estuaires et réservoirs. Thèse de docteur de l'INPG, 1987, p.173.

Sheng Y. and C. Villaret (1989). Modelling the effects of suspended sediment stratification on bottom exchange processes. *J. G. Res.*, **94** (10), p 429-444.

Thorn M.F.C. (1981). Physical processes of siltation in tidal channels. Proc. Hydraulic Modelling Applied to Maritime Engineering Problems, ICE, London, 47-55.